Seasonal Variation of the Indonesian Throughflow in Makassar Strait

TOSHIAKI SHINODA

Naval Research Laboratory, Stennis Space Center, Mississippi

WEIQING HAN

Department of Atmospheric and Oceanic Sciences, University of Colorado, Boulder, Colorado

E. JOSEPH METZGER AND HARLEY E. HURLBURT

Naval Research Laboratory, Stennis Space Center, Mississippi

(Manuscript received 7 July 2011, in final form 7 February 2012)

ABSTRACT

The seasonal variation of Indonesian Throughflow (ITF) transport is investigated using ocean general circulation model experiments with the Hybrid Coordinate Ocean Model (HYCOM). Twenty-eight years (1981–2008) of $^1/_3°$ Indo-Pacific basin HYCOM simulations and three years (2004–06) from a $^1/_{12}°$ global HYCOM simulation are analyzed. Both models are able to simulate the seasonal variation of upper-ocean currents and the total transport through Makassar Strait measured by International Nusantara Stratification and Transport (INSTANT) moorings reasonably well. The annual cycle of upper-ocean currents is then calculated from the Indo-Pacific HYCOM simulation. The reduction of southward currents at Makassar Strait during April–May and October–November is evident, consistent with the INSTANT observations. Analysis of the upper-ocean currents suggests that the reduction in ITF transport during April–May and October–November results from the wind variation in the tropical Indian Ocean through the generation of a Wyrtki jet and the propagation of coastal Kelvin waves, while the subsequent recovery during January–March originates from upper-ocean variability associated with annual Rossby waves in the Pacific that are enhanced by western Pacific winds. These processes are also found in the global HYCOM simulation during the period of the INSTANT observations. The model experiments forced with annual-mean climatological wind stress in the Pacific and 3-day mean wind stress in the Indian Ocean show the reduction of southward currents at Makassar Strait during October–November but no subsequent recovery during January–March, confirming the relative importance of wind variations in the Pacific and Indian Oceans for the ITF transport in each season.

1. Introduction

The Indonesian Throughflow (ITF) is an important part of the global thermohaline (''conveyor belt'') and wind-driven circulation carrying upper-ocean waters from the Pacific to the Indian Ocean. Since the water in the western tropical Pacific is warmer and fresher than the water in the Indian Ocean, the ITF transport impacts the temperature and salinity in the Indian Ocean as well as in the Indonesian seas. The ITF also contributes to maintaining upper-ocean circulations in the Indo-Pacific regions, including the South Equatorial Current in the Indian Ocean, the Agulhas Current, and the East Australian Current (e.g., Tilburg et al. 2001; Lee et al. 2002). Furthermore, global coupled model simulations (Schneider 1998; Song et al. 2007) suggest that the variation of ITF transport has a significant impact on tropical and global climate variability, such as the El Niño–Southern Oscillation (ENSO) and the Indian Ocean dipole (IOD) (Saji et al. 1999).

Despite the importance of ITF transport to the global ocean circulation and climate variability, there were few measurements in the Indonesian seas until recently. Hence, the total ITF transport was estimated based on limited measurements made at several key ITF passages for relatively short periods in different years (Murray

Corresponding author address: Toshiaki Shinoda, Naval Research Laboratory, Stennis Space Center, MS 39529.
E-mail: toshiaki.shinoda@nrlssc.navy.mil

DOI: 10.1175/JPO-D-11-0120.1

and Arief 1988; Molcard et al. 2001; Cresswell et al. 1993; Molcard et al. 1996; Gordon et al. 1999).

The International Nusantara Stratification and Transport (INSTANT) program was thus designed to directly measure ITF structure and variability at the major inflow and outflow passages in the Indonesian seas simultaneously (Sprintall et al. 2004). The comprehensive measurements during 2004–06 provided excellent datasets to estimate the mean and variability of ITF transport and to validate numerical model experiments, which can be used to understand processes relevant to ITF transport variations.

During the INSTANT program, a prominent seasonal variation was observed to occur at Makassar Strait, which carries ~80% of the total ITF transport (Gordon et al. 2008; see also Fig. 2). While the 3-month mean total ITF transport was always southward (from Pacific to Indian Ocean) during the entire period of the INSTANT observations, a significant reduction in southward transport during May and November was evident. Gordon et al. speculated that these reductions result from generation of the Wyrtki jet (Wyrtki 1973) and the propagation of Kelvin waves along the coasts of Sumatra and Java, such as observed and modeled during May 1997 (Sprintall et al. 2000). The possible influence of the Wyrtki jet on circulations in the Indonesian seas during these seasons is also suggested in other modeling and observational studies (e.g., Clarke and Liu 1993; Masumoto and Yamagata 1993; Potemra et al. 2002; Wijffels and Meyers 2004; Sprintall et al. 2009). However, these studies do not explicitly demonstrate the propagation of anomalous upper-ocean currents from the eastern Indian Ocean near the equator to Makassar Strait.

The importance of Pacific wind variability to seasonal variation in the ITF is suggested by Potemra (1999), based on a series of numerical model experiments. The model experiments that exclude and include Pacific wind variation demonstrate the importance of annual Rossby waves in the equatorial Pacific to the ITF seasonal variation. However, these model simulations and their analysis were performed prior to the INSTANT measurements, and the available observational data were not sufficient to validate the model results. For example, the seasonal cycle of ITF transport discussed in Potemra does not include a semiannual cycle like that observed at Makassar Strait during the INSTANT period.

The structure of the ITF and its total transport, derived from INSTANT observations, were recently compared with those from a state-of-the-art global eddy-resolving ocean circulation model experiment (Metzger et al. 2010). The 1/12° global Hybrid Coordinate Ocean Model (HYCOM) was integrated during the INSTANT period (2004–06) with 3-h atmospheric forcing. The model was able to simulate ITF total transport as well as transports at individual straits reasonably well. However, these analyses focus mainly on the evaluation of model performance in simulating the ITF, and the physical processes that control ITF variability have not been thoroughly examined.

In this paper, we investigate dynamical roles of the Pacific and Indian Oceans in determining the seasonal cycle of ITF transport through Makassar Strait and use the comprehensive observations from the INSTANT program to verify the results. In this investigation, we have used long integrations (28 years) with relatively coarse-resolution (1/3°) Indo-Pacific basin HYCOM and three years during the INSTANT period from an eddy-resolving (1/12°) global HYCOM simulation. The long integration of Indo-Pacific HYCOM allows us to obtain a climatological annual cycle so that common processes acting in most years can be identified. The eddy-resolving global HYCOM experiment, which can well represent complex bathymetry in the Indonesian Seas, is used to confirm processes found in the Indo-Pacific HYCOM by using case studies during the period of the INSTANT observations. Unlike most previous analyses, this study provides an explicit description of large-scale upper-ocean velocity variation associated with the ITF seasonal cycle. Particular emphasis is given to the relative importance of wind variations over the Pacific and Indian Oceans in controlling the ITF variation during each season. An additional model experiment, in which winds over the Pacific are set to the long-term mean climatology, is conducted to isolate the contribution of Pacific wind variation to the ITF seasonal cycle.

2. Model experiments

As the general description of HYCOM (Bleck 2002; Chassignet et al. 2003) and the description of specific HYCOM experiments used in this study (Han et al. 2010; Hurlburt et al. 2011) are detailed in other papers, the aspects most relevant to the present study are briefly described in this section.

HYCOM is a community ocean model with a generalized vertical coordinate (http://www.hycom.org). The hybrid coordinate is isopycnal in the open stratified ocean but smoothly reverts to a terrain-following coordinate in the shallow coastal regions and to pressure coordinates ($\sim z$ levels) in the mixed layer and/or unstratified seas (Bleck 2002; Chassignet et al. 2003). In this study, we use 28 years of output from an Indo-Pacific basin HYCOM experiment with horizontal resolution of 1/3° and a global HYCOM experiment with equatorial resolution of 1/12°. The integration of global HYCOM starts from 2003 and covers the entire period of the INSTANT observations.

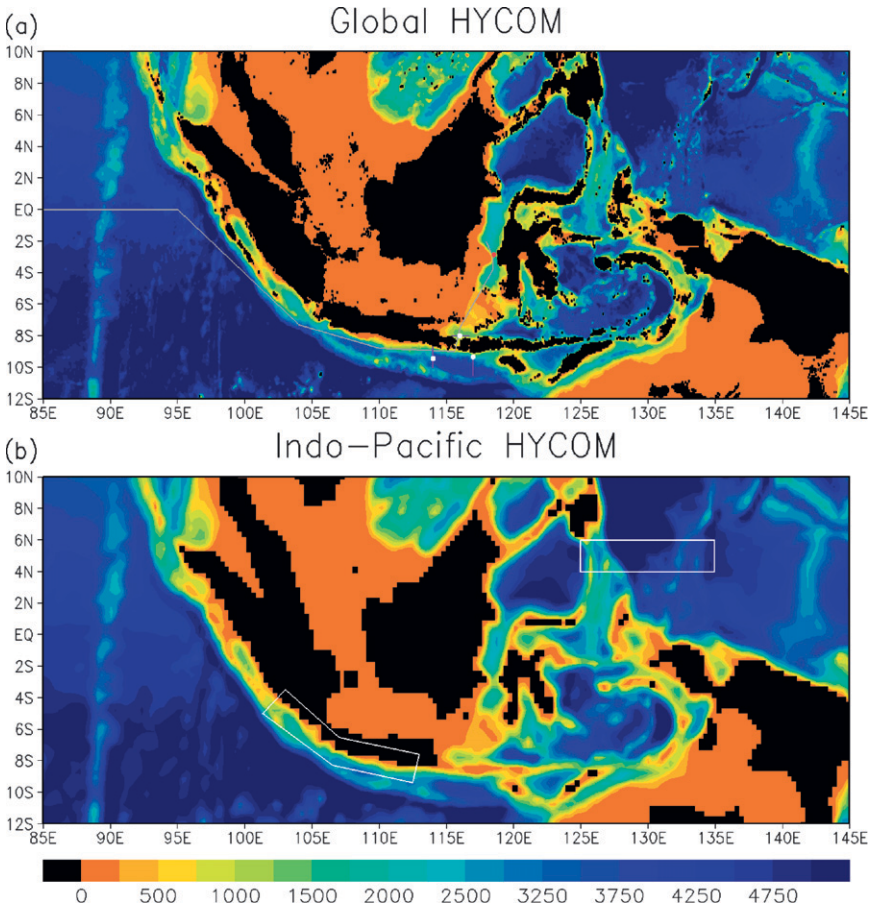

FIG. 1. Topography (m) for (a) 1/12° global HYCOM and (b) Indo-Pacific basin HYCOM for the area of the Indonesian seas. A red mark in (a) indicates the location of INSTANT moorings in Makassar Strait (2.86°S, 118.53°E: the center between the two moorings). Gray solid lines in (a) are used for Figs. 5e and 6e; purple lines (114°, 116°, and 117°E) and the white marks on the lines are used for Fig. 6 (see text and the figure captions for details); and boxes of white lines in (b) are used for Fig. 11.

The Indo-Pacific HYCOM experiment used in this study is described in Han et al. (2010). HYCOM is configured to the Indo-Pacific basin (55°S–55°N, 30°E–70°W) with 0.33° × 0.33° horizontal resolution and 20 layers in the vertical. Bottom topography data are obtained from ETOPO5 with 2° × 2° smoothing (Fig. 1). The southern and northern boundaries are closed and 5° wide buffer zones are used to relax model temperature and salinity fields to Levitus climatology.

The Indo-Pacific HYCOM was spun up from a state of rest for 30 years using Comprehensive Ocean–Atmosphere Data Set (COADS) monthly climatology fields and then integrated using 3-day-mean 40-yr European Centre for Medium-Range Weather Forecasts Re-Analysis (ERA-40) forcing fields for the period 1958–2001, the period for which ERA-40 fields are available. Restarting from 1 January 2000, the experiment was extended from 2000 to 2008 using 3-day mean winds from the Quick Scatterometer (QuikSCAT), net longwave and shortwave radiation from the International Satellite Cloud Climatology Project flux (ISCCP-FD) (Zhang et al. 2004), air temperature and specific humidity from the National Centers for Environmental Prediction–National Center for Atmospheric Research (NCEP–NCAR) reanalysis (Kalnay et al. 1996), and Climate Prediction Center (CPC) Merged Analysis of Precipitation (CMAP) pentad precipitation (Xie and Arkin 1996). In this study, we analyzed the model output for the period 1981–2008, when many satellite observations as well as in situ data in the tropics are included in the reanalysis that is used for surface forcing fields.

The global HYCOM experiment used in this study is the same as one of the experiments described in Hurlburt et al. (2011) (experiment 18.2 in their Table 1). We use

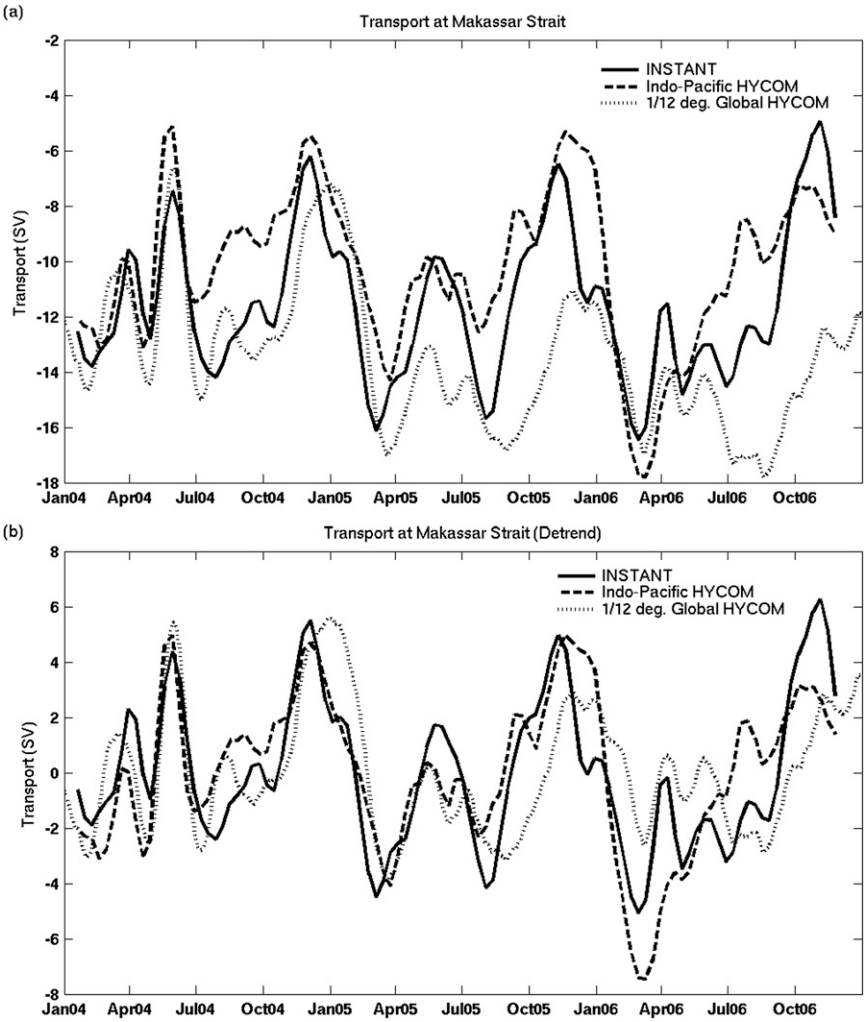

FIG. 2. (a) Total transport (Sv) at Makassar Strait during 2004–06 from the INSTANT moorings (solid line), Indo-Pacific basin HYCOM (dashed line), and 1/12° global HYCOM (dotted line). Negative transport is southward. A 30-day running filter has been applied to all time series. (b) As in (a), but the linear trends are removed and means are subtracted.

the version of global HYCOM with horizontal resolution of $1/12.5°\cos(\text{lat}) \times 1/12.5°$ (latitude × longitude) with 32 layers in the vertical. As described in detail by Metzger et al. (2010), the model topography datasets were derived from the Naval Research Laboratory 2′ digital Bathymetric Data Base 2 (DBDB2) with substantial hand editing based on a combination of navigational charts and scientific literature (Fig. 1).

The global HYCOM simulation was spun up for 10 years with climatological atmospheric forcing fields derived from ERA-40. Then the model was integrated with archived operational forcing from the Navy Operational Global Atmospheric Prediction System (NOGAPS) (Rosmond et al. 2002) for the period 2003–10, but with the long-term annual mean replaced by the long-term mean from ERA-40. Wind speed was corrected using a monthly climatology from QuikSCAT (Kara et al. 2009). The model output for the period of the INSTANT observations (2004–06) is analyzed. It should be noted that the global HYCOM experiment used in Metzger et al. (2010) is not exactly the same as the one used in this study, in which the surface forcing, model code, and topography dataset were further improved (Hurlburt et al. 2011).

While the coarse resolution of the Indo-Pacific basin HYCOM makes it possible to perform a long integration, the model does not adequately resolve the individual passages in the Indonesian Seas (Fig. 1). For example, a number of small islands between Sulawesi and the Halmahera Sea are absent. This bathymetric configuration around Makassar Strait might allow a

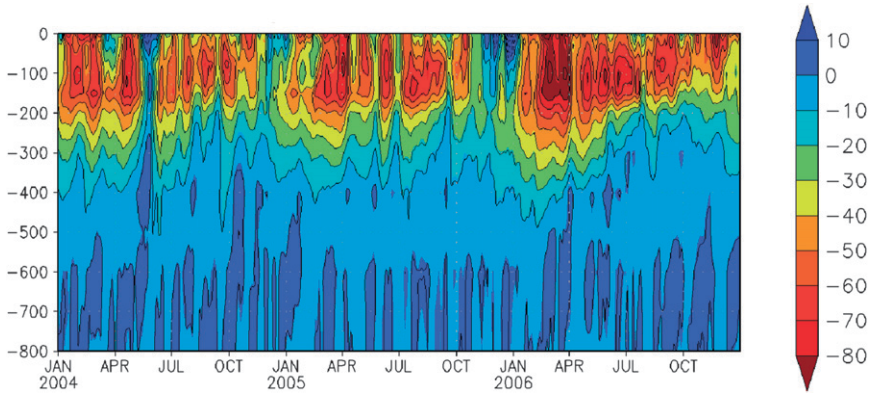

FIG. 3. Along-channel velocity (cm s^{-1}) at Makassar Strait during 2004–06 from the Indo-Pacific basin HYCOM simulation.

stronger South Pacific contribution to the throughflow than that shown in the observations. Also, some of the islands along the Nusa Tengarra are subsurface, which might affect the penetration of coastal Kelvin waves into the Indonesian seas. However, as shown in the next section, the model simulation of the ITF transport agrees well with observations and high-resolution model results, suggesting that major physical processes controlling the ITF seasonal variation may be well represented by the 1/3° coarse-resolution model.

3. Results

a. *Comparison with INSTANT observations*

The variation of the ITF in HYCOM simulations is compared with INSTANT observations at Makassar

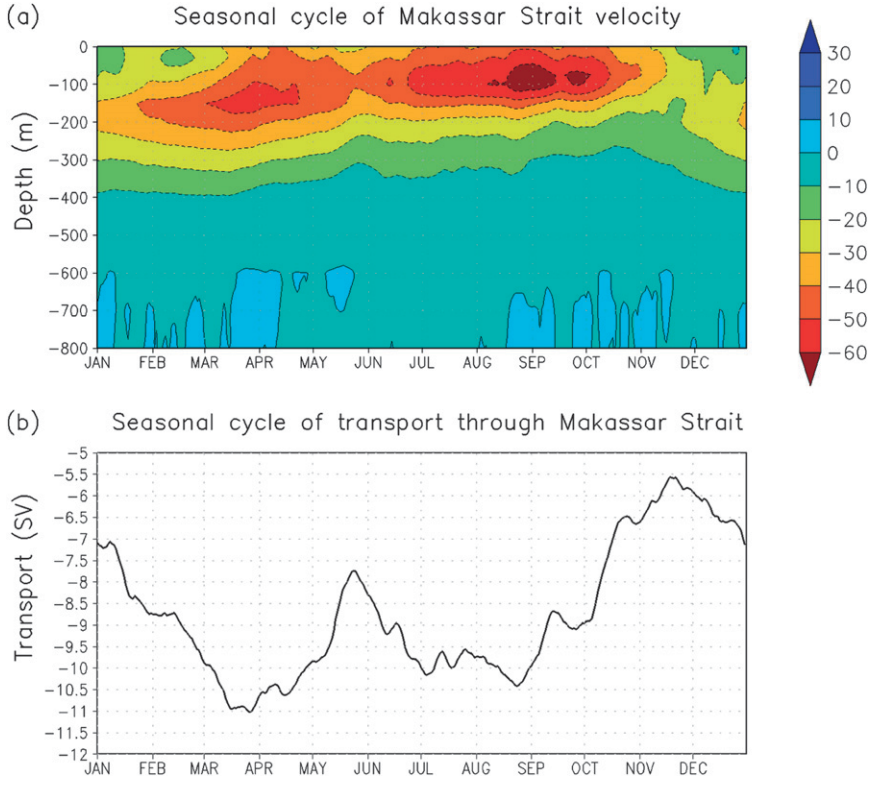

FIG. 4. Seasonal cycle of (a) along-channel velocity (cm s^{-1}) and (b) total transport (Sv) at Makassar Strait, based on a 28-yr mean from the Indo-Pacific HYCOM simulation: the standard deviation of the transport is 1.52 Sv.

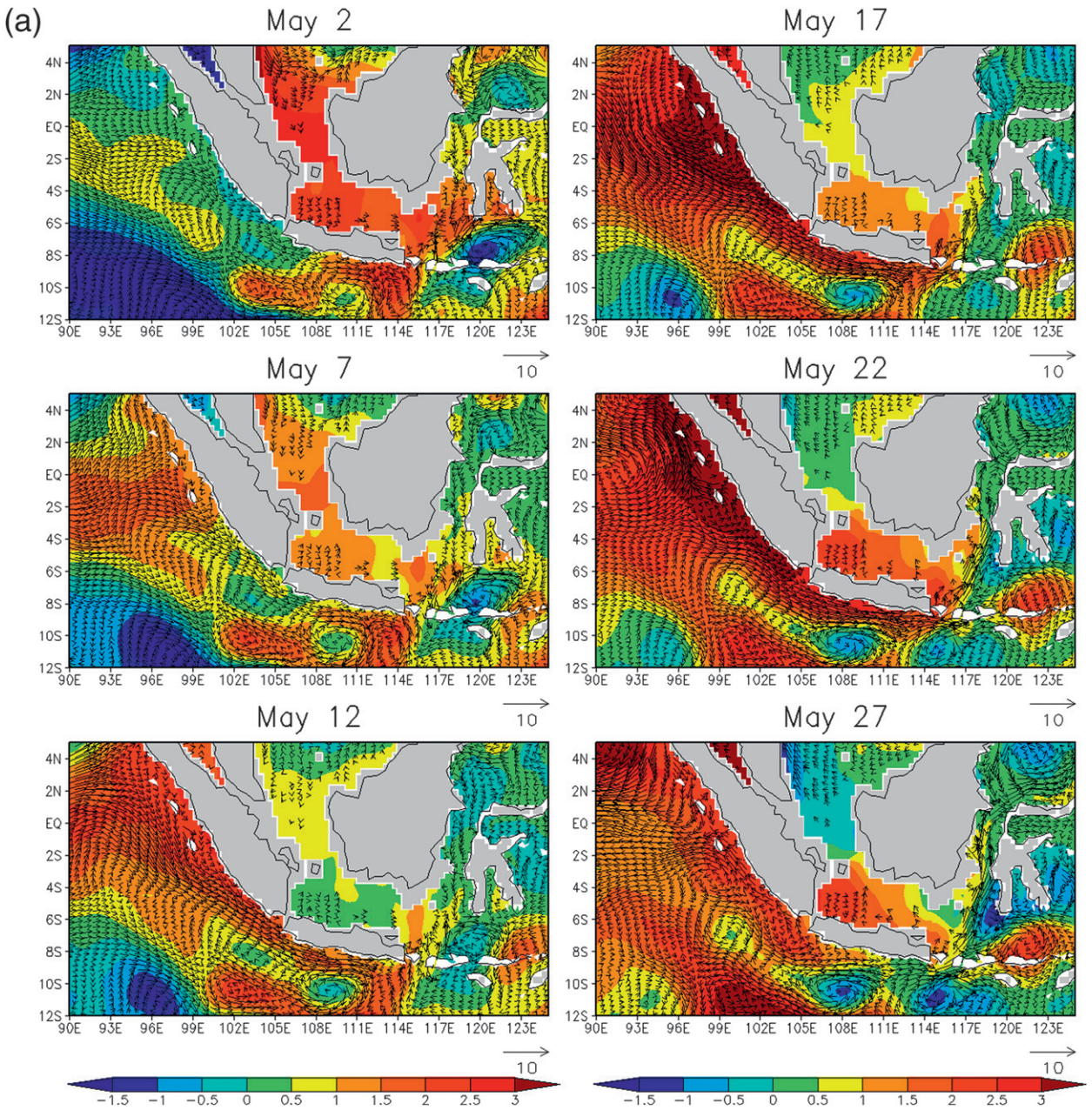

FIG. 5. (a) Anomaly snapshots of SSH (shading, cm) and upper-ocean (average over 50–150-m depth) velocity (vectors, cm s^{-1}) from the annual cycle relative to the April–June mean derived from the Indo-Pacific basin HYCOM simulation. The snapshots cover 2–27 May. Gray shading indicates land grid points in the model. (b) As in (a) but for SSH (shading, cm) anomalies from satellite altimeter data and wind stress (vectors, N m^{-2}) anomalies used to force the model. The color scale is different from (a). (c) SSH (shading; m) and upper-ocean (average over 50–250-m depths) velocity (vectors) anomalies during 9–30 May 2004 relative to the mean of April–June 2004 from the global HYCOM simulation. A 30-day running filter has been applied to the time series. (d) As in (c) but for a smaller domain and the period 17–27 May 2004. (e) Alongshore and along-strait velocity (shading) and SSH (contour) anomalies along the gray solid line shown in Fig. 1. Both alongshore and along-strait velocities are defined as the velocity component along the gray line. Contour interval is 0.5 cm; the dashed contour line indicates negative values and blue solid lines indicate the phase line of 2.5 m s^{-1}.

Strait, which is the primary inflow passage, carrying ~80% of the total ITF transport (Gordon 2005; Gordon et al. 2008). Figure 2a shows the time series of total transport at Makassar Strait estimated from HYCOM simulations and two INSTANT mooring observations located at 2°51.90′S, 118°27.30′E and 2°51.50′S, 118°37.70′E. The mean transport during this period from the Indo-Pacific HYCOM [−10.2 Sv (Sv ≡ 10^6 m^3 s^{-1})] and global

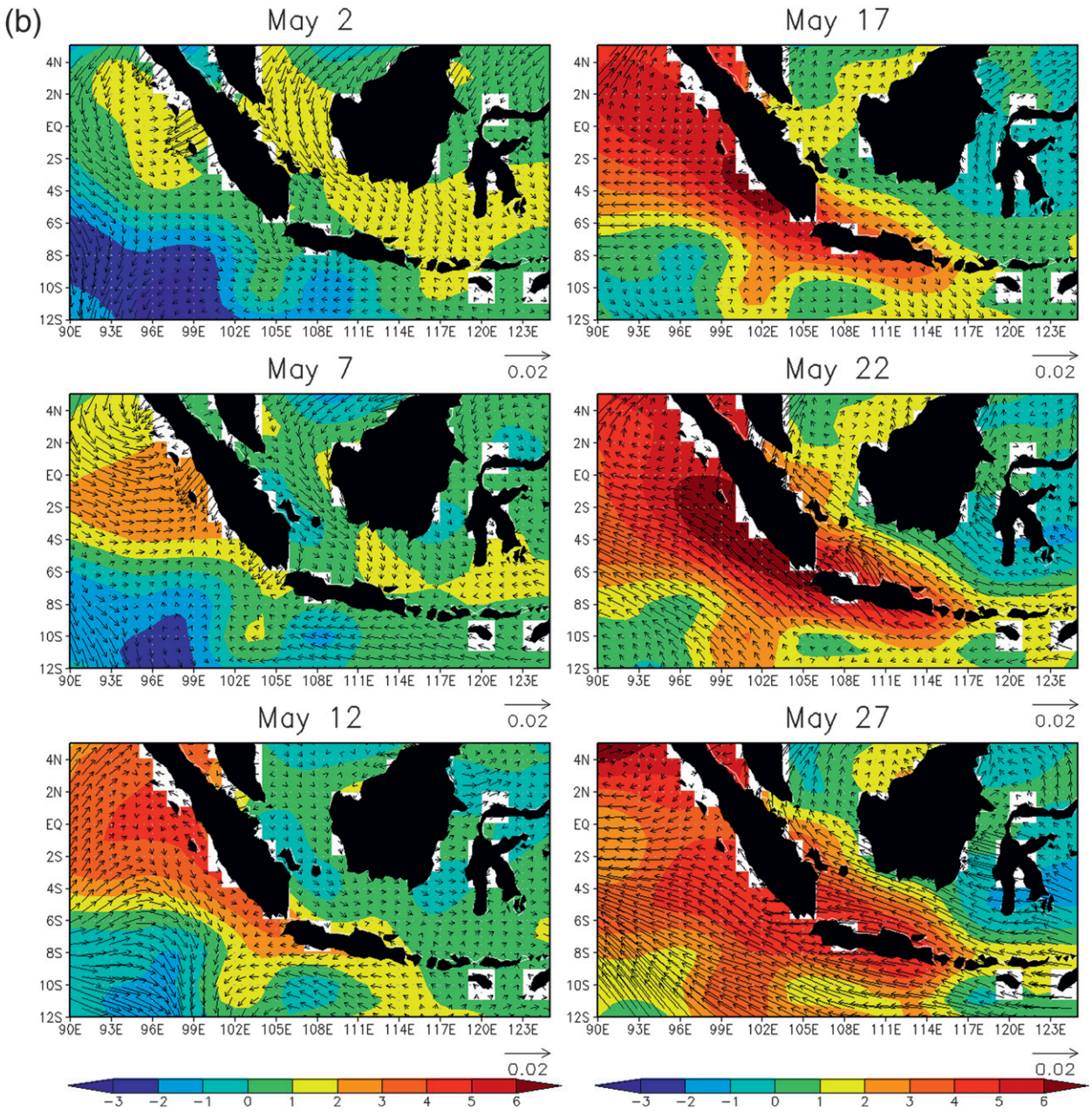

FIG. 5. (*Continued*)

HYCOM (−13.5 Sv) simulations agree well with the observations (−11.6 Sv). However, the transport from the global HYCOM simulation shows an apparent increasing trend of southward transport. To compare only the transport variations, we removed the linear trends and the mean from each time series (Fig. 2b). The seasonal variations of the transport from both the Indo-Pacific and global HYCOM simulations are quite similar to those from the INSTANT observations, where a significant reduction in southward transport is found during April–May and October–November. In addition, the rapid increase of the southward transport during February–March is evident and is simulated by both models. It should be noted that the mean net transport of the global HYCOM simulation, shown in Fig. 2a, is closer to that observed than the model transport given in Metzger et al. (2010) (see their Fig. 5). This is due to a combination of the improvement in the model topography, surface forcing, and model code, but it is difficult to identify the relative importance of these changes.

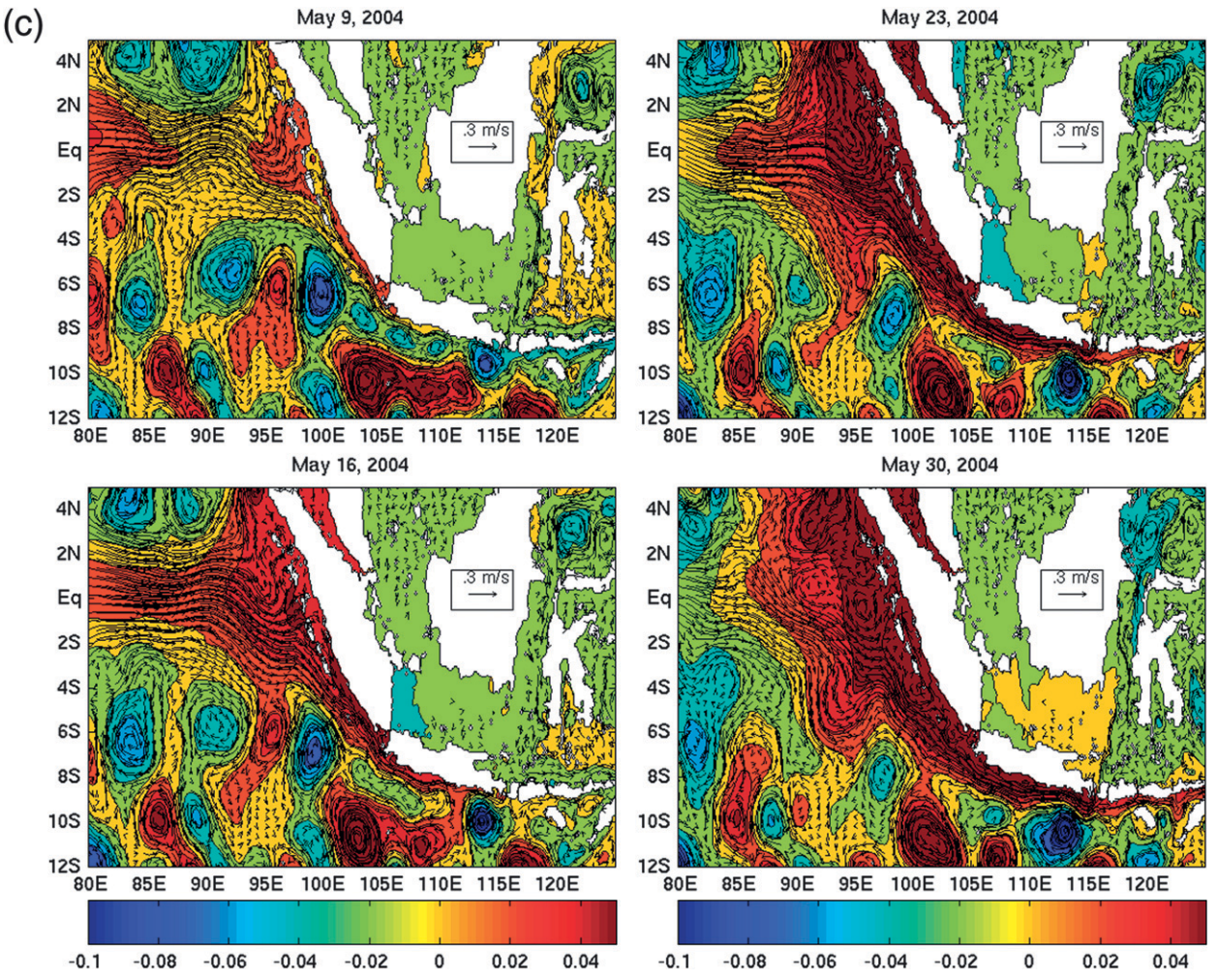

FIG. 5. (*Continued*)

Figure 3a displays the along-channel velocity at Makassar Strait from the Indo-Pacific HYCOM. The velocity is calculated from the average of the two grid points (2.86°S, 118.44°E and 2.86°S, 118.77°E) closest to the mooring locations. The simulated along-channel velocity is quite similar to observations [see Fig. 2 in Gordon et al. (2008)]. The maximum along-channel velocity is found around depths of 100–200 m for both the model and observations. The along-channel velocity in the upper ocean is stronger during 2006 in both model and observations. However, there are some notable differences. For example, the maximum velocity around 150 m during July 2006 is underestimated by the model. Also, the variation below 600 m in the model is not similar to observations. A weak northward current below 600 m is often found in the model, whereas the observed current around this depth is southward most of the time. Nevertheless, the model reproduces the seasonal evolution of upper-ocean velocity and total transport at the INSTANT mooring sites reasonably well: thus, it provides a tool for examining physical processes that control the ITF seasonal variation.

To examine common processes acting in most years, the seasonal cycle is calculated using 28 years of output from the Indo-Pacific HYCOM experiment. The seasonal cycle of the along-channel velocity and total transport at Makassar Strait are shown in Fig. 4. A semiannual cycle of along-channel velocity in the 50–150-m depth range is clearly evident. The maximum velocity is found during August–September and a secondary maximum is evident during April–May. A significant reduction in southward velocity is found during May and November. Associated with the current variations in the upper ocean, a semiannual variation in total transport is also clearly evident (Fig. 4b). Southward transport is reduced during May and November and rapidly recovers during January–March. These ITF seasonal variations are consistent with the transport observed during the INSTANT period,

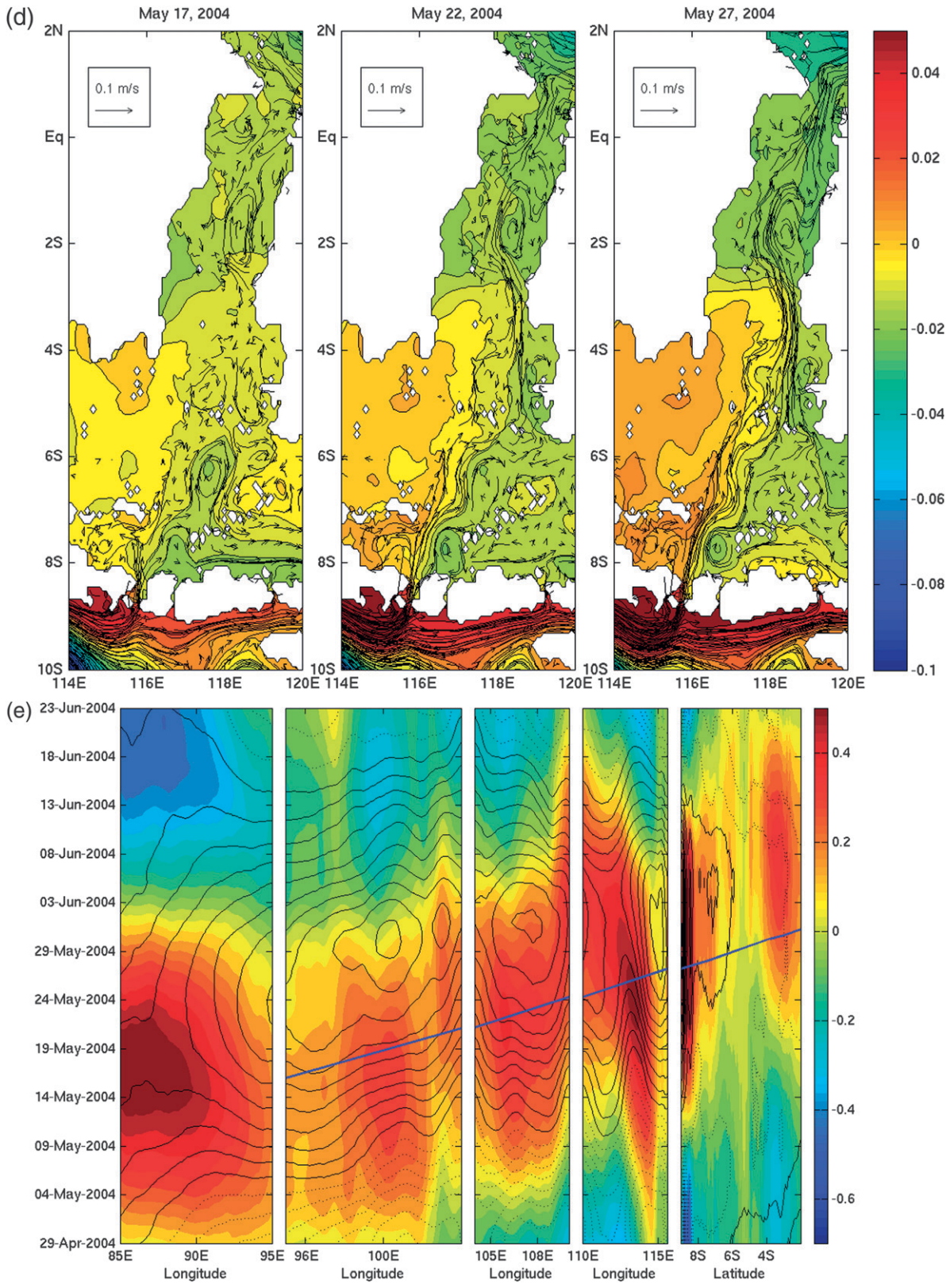

FIG. 5. (*Continued*)

although there are some significant deviations from the climatological seasonal cycle each year.

b. Processes that control the ITF seasonal cycle

In the previous section, it was shown that both the INSTANT observations and long-term integrations of Indo-Pacific HYCOM have a similar seasonal cycle in ITF transport. In this section, processes that control the ITF variation are investigated for each period of the year when a prominent change in ITF transport is evident in the climatological seasonal cycle. Specifically, we discuss processes during April–May and October–November when a significant decrease in southward transport occurs and also those during January–March recovery of a strong southward current.

1) APRIL–MAY

Figure 5a shows anomalous sea surface height (SSH) and currents averaged over 50–150-m depths during 2–27 May from the seasonal cycle of Indo-Pacific HYCOM. Anomalies are calculated by subtracting the April–June mean. During early May equatorial eastward currents develop in the eastern Indian Ocean, which are associated with the increase in SSH near the eastern boundary. This eastward current is often referred to as the Wyrtki jet that is generated by the equatorial westerlies during this season (Wyrtki 1973). SSH anomalies continue to increase at the eastern boundary and propagate along the coast of Sumatra and Java during mid-May. These high SSH anomalies near the coast are associated with an alongshore velocity that is eastward near Lombok Strait (8°S, 115°E). Although a significant portion of the current and SSH anomalies passes across Lombok Strait, some signals propagate northward through Lombok Strait in late May and generate anomalous northward currents at Makassar Strait. It takes approximately one month for the anomalies associated with the Wyrtki jet to propagate from the eastern boundary near the equator to Makassar Strait—consistent with the phase speed of a Kelvin wave in this region (e.g., Sprintall et al. 2000).

The SSH anomaly pattern during this season is also examined using satellite altimeter data. The anomaly is calculated from the mean seasonal cycle of SSH over the period 1993–2009 using the daily $1° \times 1°$ gridded altimetry product obtained from Archiving, Validation, and Interpretation of Satellite Oceanographic data (AVISO). A similar variation in SSH anomalies during this season is found in the satellite altimeter data (Fig. 5b). However, the amplitude of the SSH variation is larger than in the model. This difference is partly attributed to the difference in the analysis period. The SSH variation in the Indo-Pacific HYCOM for the period 1993–2008 is shown to be ~50% larger than that in Fig. 5a (not shown), but it is still significantly weaker than observations.

Figure 5b also shows the anomalous wind stress during this period. During late May southeasterlies along the coast of Sumatra and Java develop. This anomalous wind stress near the coast generates coastal upwelling or reduces downwelling. Hence, the local winds in this region tend to reduce the SSH and alongshore current anomalies. The maximum SSH anomalies are found around 0°–6°S near the coast of Sumatra on 20 May in both observations and model. These SSH anomalies around this area are considerably reduced on 27 May.

Figure 5c shows the SSH and upper-ocean (50–250-m depths) current anomalies during 24 April–15 May 2004 from the global HYCOM simulation. A prominent reduction in southward ITF transport was observed during this period (Fig. 2). Propagation of the SSH and alongshore velocity similar to that in the climatological seasonal cycle obtained from the Indo-Pacific HYCOM is evident. Also, the development of a northward current anomaly near Makassar Strait in early to mid May is clearly demonstrated in the SSH and current anomaly map for a smaller subregion (Fig. 5d). Large positive SSH anomalies near Lombok Strait are found on 17 May. As the SSH anomalies increase during this period, strong anomalous northward currents at Lombok Strait are generated. Subsequently, these currents extend farther northward and on 27 May strong anomalous currents are evident at Makassar Strait.

The propagation of coastal Kelvin waves and their influence on the ITF transport are further demonstrated by showing the velocity and SSH fields along the path of the Kelvin wave. Figure 5e shows the evolution of the alongshore velocity and SSH along the equator in the eastern Indian Ocean, the coasts of Sumatra and Java, and from Lombok to Makassar Straits (the gray solid line shown in Fig. 1). Propagation of SSH and velocity along the coastline and through the Lombok and Makassar Straits is evident. Also, the propagation speed is consistent with the phase velocity of the first baroclinic-mode free Kelvin wave over the Indian Ocean, which is ~2.6 m s^{-1} (e.g., Moore and McCreary 1990; Han 2005). It should be noted that the propagation speed may deviate from the free Kelvin wave speed because of complex topography, such as a shallow shelf along the coast. Also, the phase speed can be modified by surface forcing (e.g., Shinoda et al. 2008).

The results indicate that the SSH and velocity are not in phase near the equator, which is not consistent with the structure of a free coastal Kelvin wave for a single baroclinic mode derived from the theory. The SSH and velocity shown in Fig. 5e, however, represent the sum of all vertical modes. This sum, together with the complexity

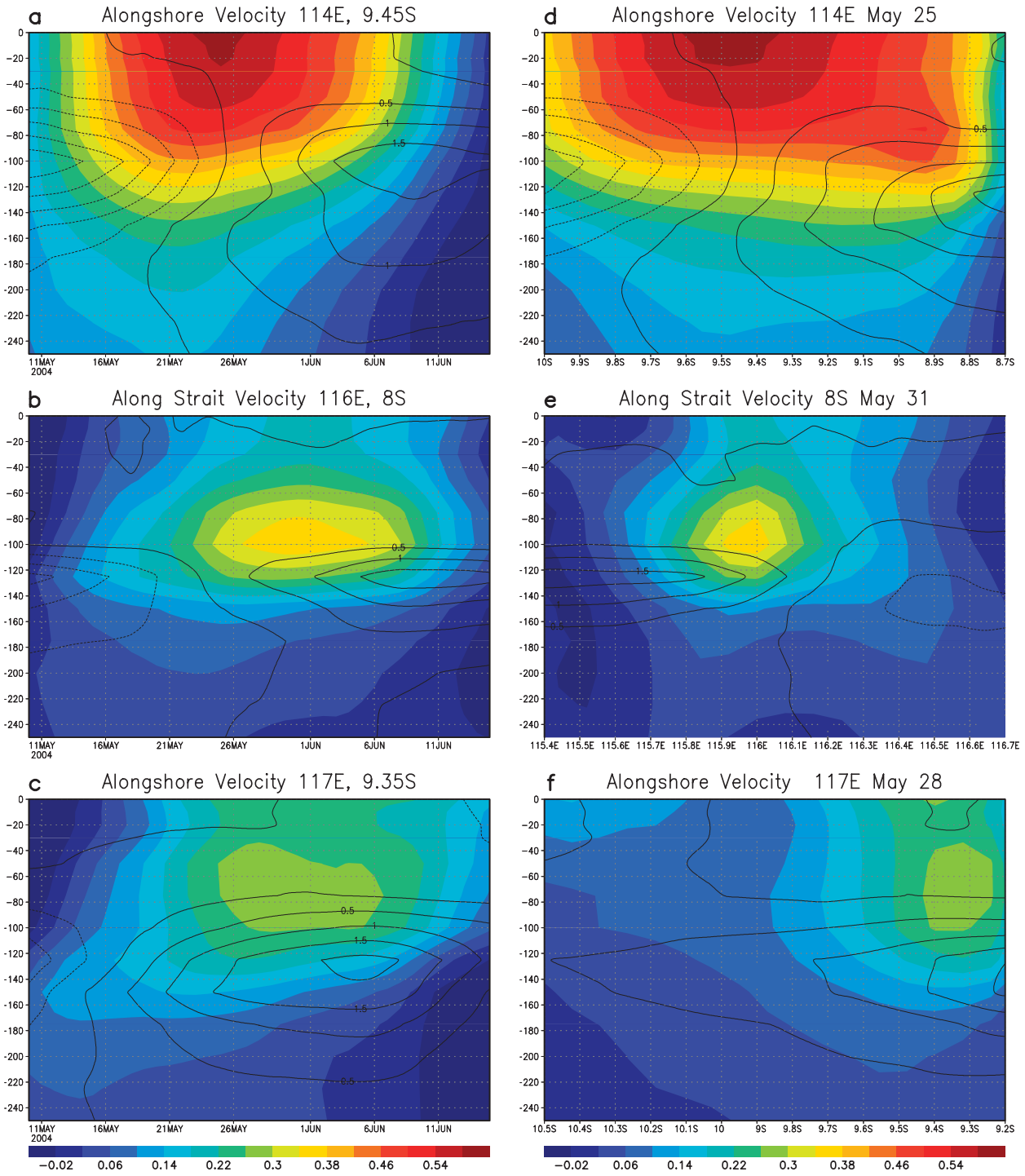

FIG. 6. (a) Time–depth plot of alongshore velocity (shading) and temperature (contoured) anomalies at 9.45°S, 114°E from the global HYCOM experiment during May 2004: contour interval is 0.5°C and dashed contours indicate negative values. (b) As in (a) but for the along-strait velocity at 8°S, 116°E and (c) as in (a) but at 9.35°S, 117°E. (d) Alongshore velocity and temperature anomalies on 25 May along the purple line at 114°E shown in Fig. 1, (e) as in (d) but for the purple line at 8°S shown in Fig. 1, and (f) as in (d) but for the purple line at 117°E shown in Fig. 1.

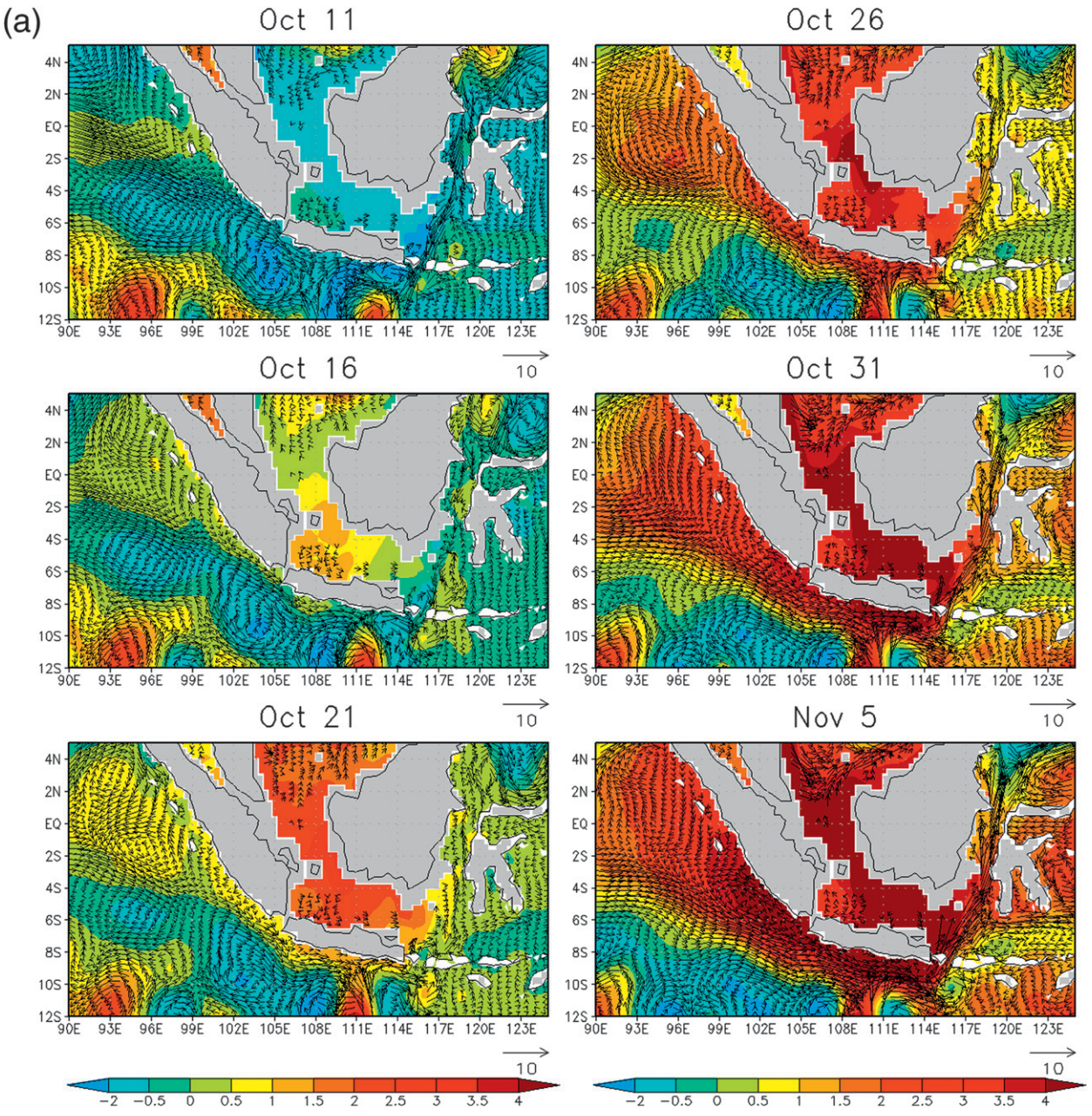

FIG. 7. (a),(b) As in Figs. 5a,b but for the period 11 Oct–5 Nov 2005 and anomalies are relative to the October–November mean. (c) As in Fig. 5c but for the period 29 Oct–19 Nov 2005 and anomalies are relative to the October–November mean. White lines are the same as the gray lines in Fig. 1a. (d) As in Fig. 5d but for the period 8–18 Nov 2005. (e) As in Fig. 5e but for the period 5 Oct–11 Dec 2005.

of topography and the lateral friction near the boundary, may produce a phase discrepancy between SSH and velocity (Yuan and Han 2006). In addition, a strong convergence in an equatorial jet near the eastern boundary may not be compensated by the divergence of meridional currents along the coast, which can be reduced by the lateral friction near the boundary. Thus, positive SSH anomalies along the coast near the equator could continue to increase when equatorial zonal current anomalies are positive.

While the overall propagation of SSH and velocity from the equatorial eastern Indian Ocean to Makassar Strait is demonstrated in Fig. 5e, the amplitude of the velocity fluctuation varies significantly along the path. For example, strong positive along-strait velocity is found at both Lombok and Makassar Straits during late May–early

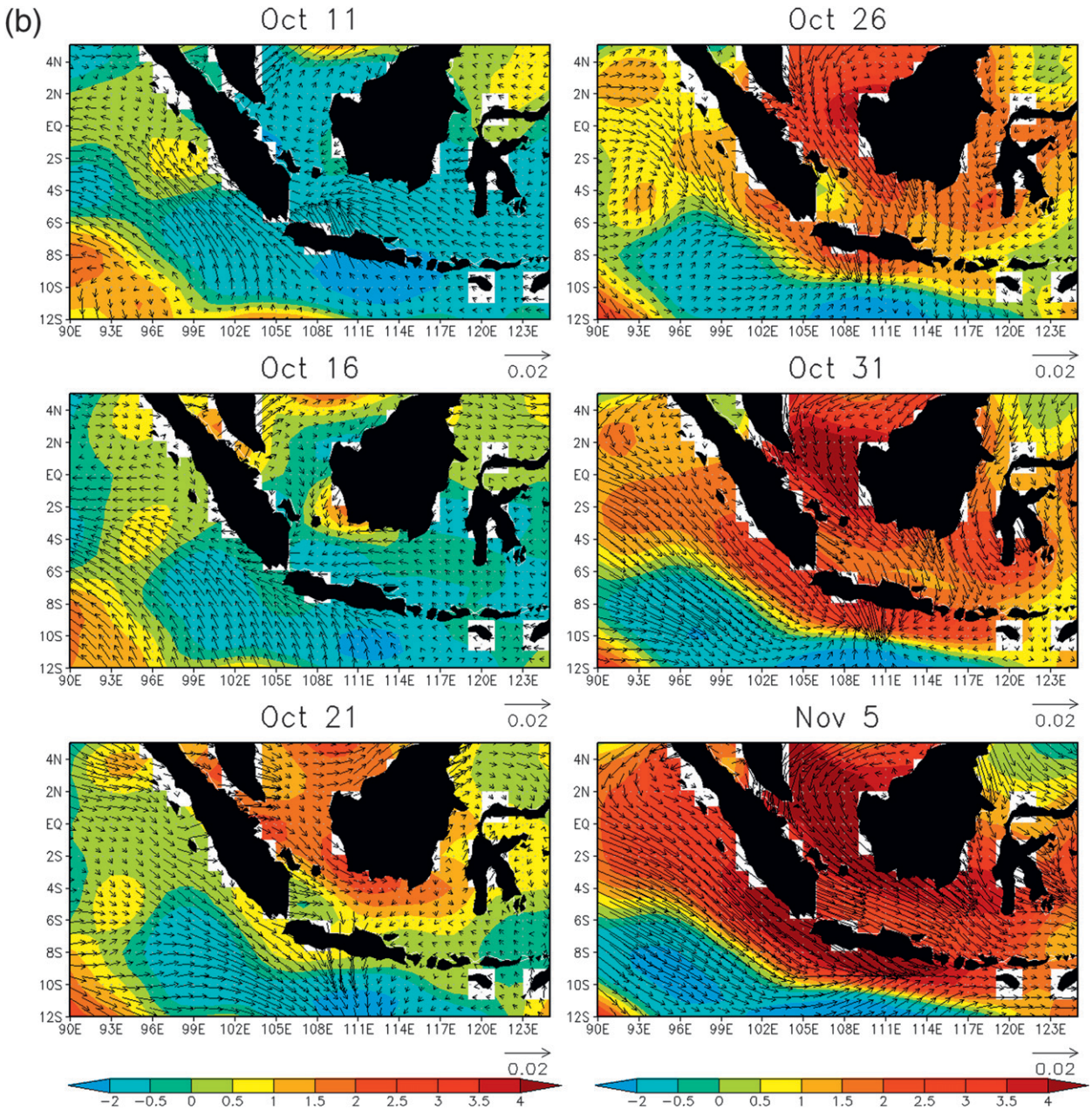

FIG. 7. (*Continued*)

June, but the velocity is much weaker between the two straits. This occurs because the horizontal scale of the currents varies substantially in the Indonesian Seas owing to the complex topography (Fig. 5d). Also, westward propagation of alongshore velocity is found around 112°–115°E. This is due to the strong cyclonic eddy near the coast, which becomes stronger and extends westward by the end of May 2004 (Fig. 5c). These eddy fields could influence Kelvin wave propagation through nonlinear interaction and thus could possibly affect the ITF transport since the alongshore velocity associated with mesoscale eddies is comparable to that of the Kelvin waves.

While Kelvin wave propagation from the coast of Java to Makassar Strait through Lombok Strait is evident in models, some of the Kelvin wave energy may cross Lombok Strait and continue propagating eastward along the Nusa Tenggara coastal waveguide (e.g., Hautala et al. 2001; Molcard et al. 2001; Sprintall et al. 2009). In fact, significant SSH anomalies near the coast east of Lombok

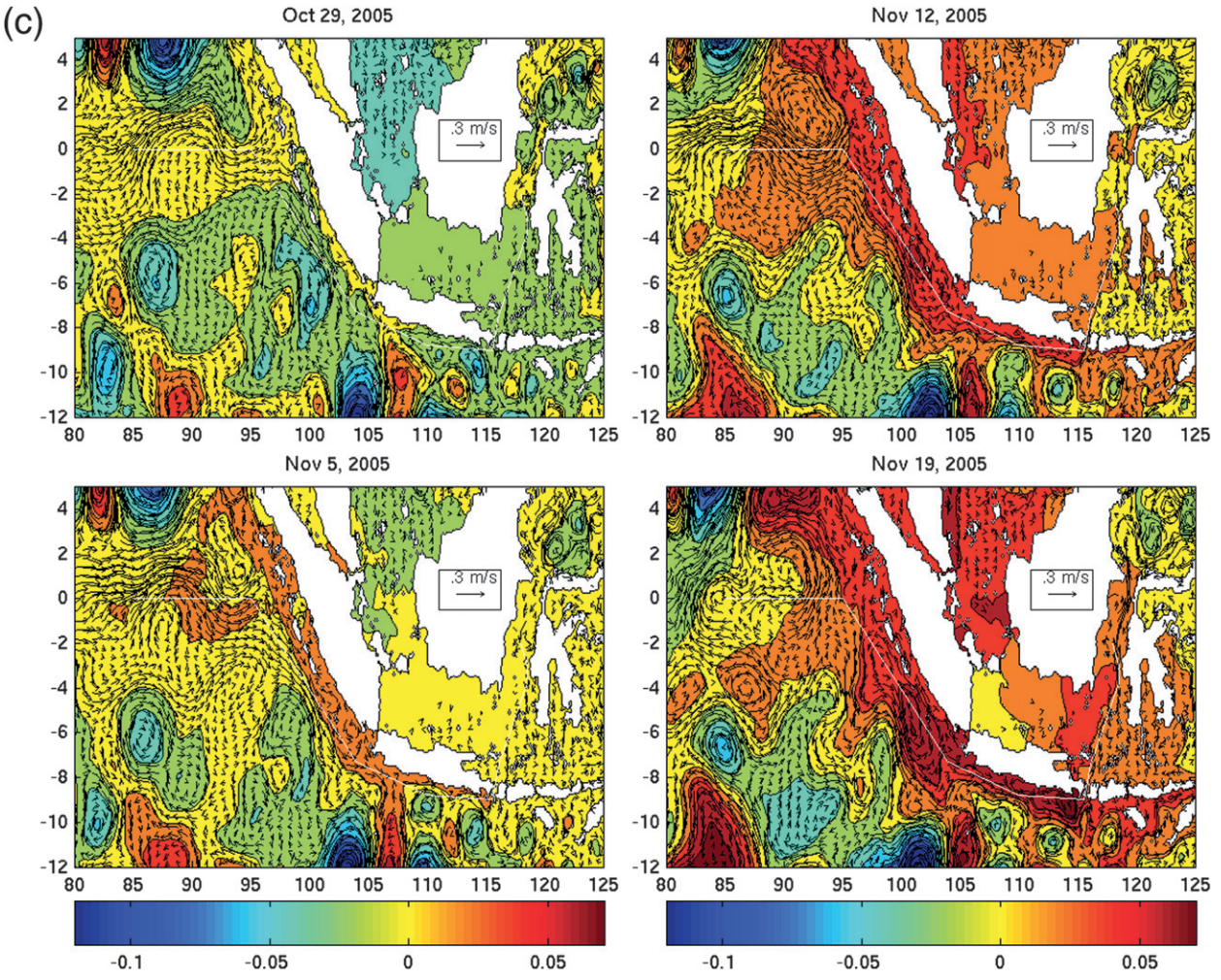

FIG. 7. (*Continued*)

Strait are evident, and their amplitude is about half of the SSH anomalies west of Lombok Strait (Fig. 5d), consistent with previous studies based on the analysis of satellite SSH observations (Syamsudin et al. 2004; Drushka et al. 2010).

We further investigate the vertical structure of velocity and temperature associated with the Kelvin wave propagation near Lombok Strait in the global HYCOM simulation. Figure 6 shows time–depth plots and meridional sections of alongshore velocity and temperature anomalies at three locations (west, east, and north of Lombok Strait, shown in Fig. 1) during May 2004 when the propagation of Kelvin waves is clearly evident. The maximum alongshore velocity of ~60 cm s^{-1} west of Lombok (9.45°S, 114°E) is found at the surface on 25 May (Figs. 6a,d). The temperature anomalies around the middle of the thermocline (depth ~100 m) vary by about 5°C, which is due to the deepening of the thermocline by ~25 m (not shown). Several days later (31 May), a velocity maximum (~37 cm s^{-1}) north of the Lombok (8°S, 116°E) is found around 100-m depth (Figs. 6b,e). At this location, the change of the temperature anomaly in the middle of the thermocline is about 3°C. East of Lombok Strait (9.35°S, 117°E) the maximum velocity occurs close to the coast at 60–80-m depth (Figs. 6c,f), which is consistent with previous studies that show downward propagation of Kelvin waves in this region (e.g., Wijffels and Meyers 2004; Drushka et al. 2010). The maximum velocity at this location is about 29 cm s^{-1}. The analysis suggests that more than half of the Kelvin wave energy along the coast of Java penetrates into the interior Indonesian seas through Lombok Strait and the rest passes across Lombok Strait. However, further quantitative discussion may not be possible since an accurate estimate of wave energy (e.g., Potemra 2001; Durland and Qiu 2003) is difficult to obtain from an eddy-resolving model because of active mesoscale and submesoscale eddies and the uncertainty of the wave period.

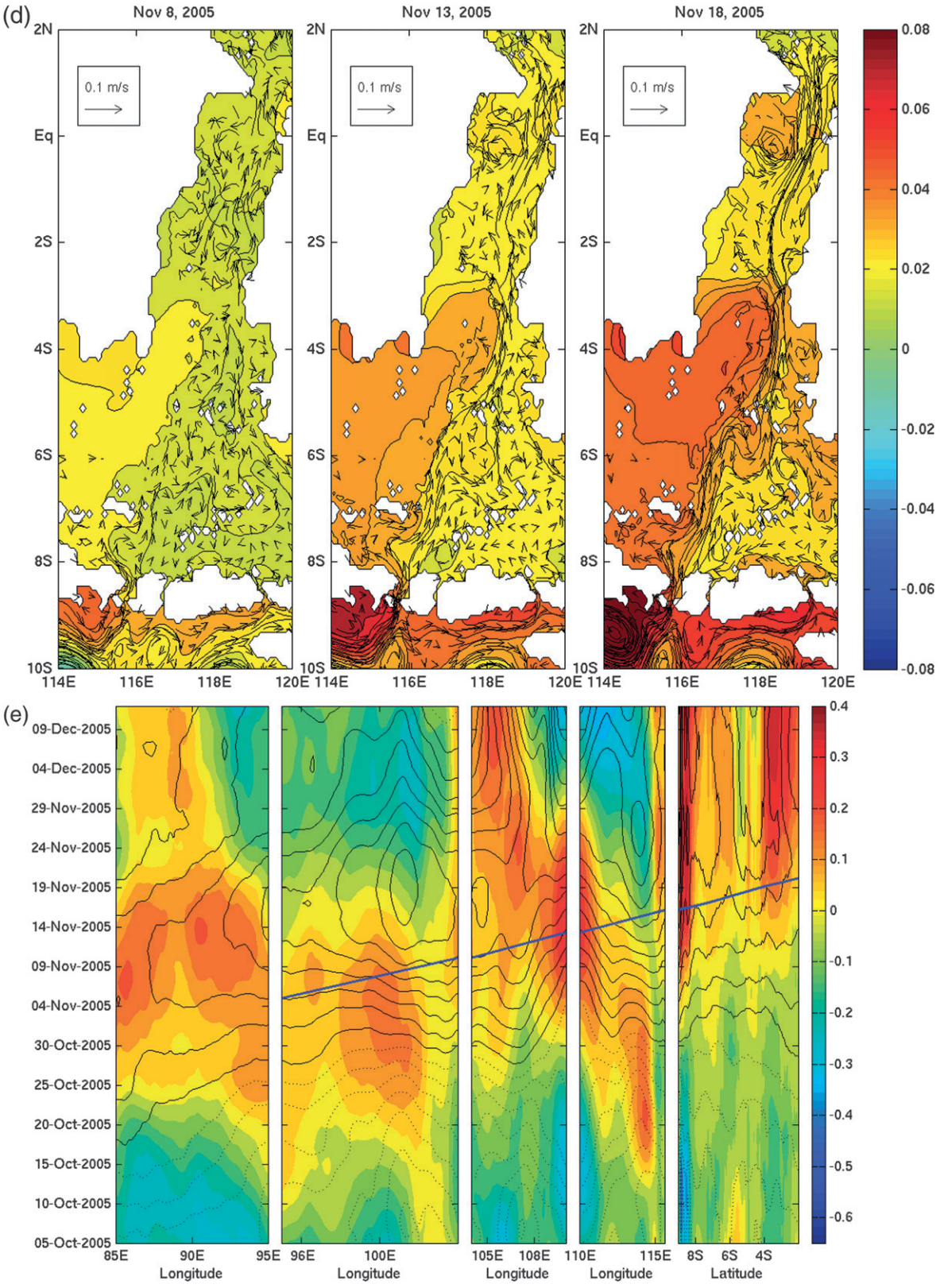

FIG. 7. (*Continued*)

2) OCTOBER–NOVEMBER

Figure 7a shows the evolution of SSH and upper-ocean current anomalies during the period 11 October–5 November. A decrease in southward transport at Makassar Strait is observed during this season. SSH and current variations are similar to those in May when eastward currents and positive SSH anomalies, associated with the Wyrtki jet, propagate along the coast of Sumatra and Java and farther to Makassar Strait through Lombok Strait. However, there are some notable differences. As the SSH anomalies propagate along the coast, they are enhanced near Java and Lombok Strait. Also, large SSH anomalies are found in the Java Sea.

Figure 7b shows SSH anomalies from satellite altimetry along with the wind stress anomalies during this period. The SSH anomalies are quite similar to those from the model simulation. During late October to early November, an equatorial westerly wind component and northwesterlies along the coast of Sumatra and Java develop, the opposite of anomalous winds along the coast during late May. The wind stress associated with northwesterlies generates coastal downwelling. Thus, the positive SSH anomalies tend to be enhanced, which is consistent with the satellite altimeter data. This enhancement by the alongshore winds could be responsible for the larger reduction in ITF transport during this season than occurred in May (Fig. 4). Also, strong anomalous winds in the Java Sea can generate large SSH anomalies during this season. The increase in SSH anomalies at the northern end of the Java Sea extends eastward and may influence the north–south pressure gradient in the southern part of Makassar Strait. Hence, the enhancement of the northward pressure gradient generated by local winds could also contribute to the ITF variation at Makassar Strait during this season (e.g., Gordon et al. 2003).

Figures 7c,d show SSH and upper-ocean current anomalies during late October to mid November 2005 from the global HYCOM simulation. Northward anomalous currents from Lombok Strait to Makassar during this period (Fig. 7d) are quite similar to those in May 2004 (Fig. 5d). However, the propagation of the SSH and current fields appears to be affected by mesoscale eddies more than during May 2004. In particular, there are several mesoscale eddies along the coast around 4°–10°S, which can interact with Kelvin waves along the coasts of Sumatra and Java. These eddies could be generated by barotropic and baroclinic instabilities due to the strong temperature and salinity gradients and strong zonal shear between the South Equatorial Current and Eastern Gyral Current (Yu and Potemra 2006). Nevertheless, the evolution of northward anomalous currents from Lombok Strait to Makassar Strait during this period (Fig. 7d) is quite similar to that in May 2004 (Fig. 5d).

Figure 7e shows the evolution of SSH and alongshore and along-strait velocity during this period along the same line used in Fig. 5e. Although the propagation of SSH and velocity from the eastern Indian Ocean to Makassar Strait are similar to that during May 2004 (Fig. 5e), both SSH and velocity fields are much noisier. In particular, velocity fields seem to be affected by several mesoscale eddies along the path of the Kelvin waves. For example, significant positive alongshore velocity is found near the coast of Java just west of Lombok Strait (110°–115°E) in late October, which is associated with cyclonic eddies (Fig. 7c). Although these velocity fields, generated by eddies, are not associated with coastal Kelvin waves, their magnitude is comparable to or larger than those associated with Kelvin waves. These eddies are enhanced and extended westward during this period (19 November), and thus the westward propagation of positive alongshore velocity is evident around 105°–115°E in Fig. 7e. Also, an anticyclonic eddy centered around 5°S, 102°E develops in mid-November. Because of this eddy, the area of significant positive alongshore velocity is shifted westward (west of the white line in Fig. 7c). Hence, the eastward propagation is not clear around this region in Fig. 7e, as the velocity fields are greatly affected by the eddy. Nevertheless, the propagation along the coasts and through straits is clear in the SSH fields, consistent with the phase speed of a Kelvin wave.

3) JANUARY–MARCH

During January–March strong southward upper-ocean currents through Makassar Strait recover, after weakening during October–November. The strong influence of Pacific Ocean variability on anomalous currents at Makassar Strait is demonstrated in Fig. 8. The influence of Indian Ocean variability, found during May and October–November, is not evident in SSH and upper-ocean current maps during this period.

Figure 8a shows the SSH and upper-ocean current anomalies relative to the seasonal mean during January–March from the Indo-Pacific HYCOM simulation. During January anomalous currents in the western Pacific around 5°N are eastward, a feature connected to the northward anomaly in currents at Makassar Strait. The reversal of the eastward current anomaly, associated with positive SSH anomalies, starts around 5°N, 135°–140°E in mid-February, and these anomalies propagate westward. The current anomalies further propagate into the Indonesian seas and generate strong anomalous southward currents through Makassar Strait. During this period, persistent positive SSH anomalies are found near the coast of Java, and thus the influence of

Indian Ocean variability on the ITF variation is not evident.

In association with the anticyclonic circulation centered around 5°N, 132°E in mid-March (Fig. 8a), an anomalous cyclonic circulation east of Mindanao is enhanced during this period, which may contribute to the anomalous westward current around 4°N through strengthening of the Mindanao Current. However, the SSH and velocity anomalies associated with Mindanao eddies are much smaller than those associated with the anticyclonic circulation around 5°N and, thus, may not be of primary importance in contributing to the ITF seasonal variation.

A similar evolution of SSH is also found in the satellite altimeter data during this period (Fig. 8b). Although the spatial pattern and time variation during this period are well simulated by the Indo-Pacific HYCOM, the amplitude of SSH anomalies is larger in the model. The significant influence of Pacific variability on the ITF is also demonstrated in the global HYCOM simulation for this season in 2005 (Figs. 8c,d). The development of positive SSH anomalies around 5°–8°N in the western Pacific associated with anomalous westward currents around 4°N is evident. As the SSH near the western boundary increases, the anomalous southward currents extend to Makassar and Lombok Straits (Fig. 8d).

The processes that generate the increase of SSH in the western Pacific north of the equator during this season are further investigated by analysis of the Indo-Pacific HYCOM simulation in the entire tropical Pacific. Figures 9a,b show longitude–time diagrams of SSH and Ekman pumping velocity anomalies over 3°–7°N, respectively. Anomalies are calculated by subtracting the annual mean. The negative wind stress curl in the eastern Pacific around 3°–7°N during boreal summer and fall (Fig. 9c) generates strong downwelling (and thus an increase in SSH), and these SSH anomalies propagate westward as Rossby waves (Fig. 9a). The simulated annual Rossby waves are consistent with previous observational studies (Meyers 1979; Kessler 1990; Potemra 1999). During January–March, downwelling Rossby waves reach the western boundary and generate the rapid increase in SSH (Fig. 9d). While this rapid SSH increase near the western boundary is associated with annual Rossby waves, their amplitude is enhanced as they propagate into the western Pacific east of the date line (Fig. 9a). In particular, during mid January–late February, SSH decreases by ~15 cm around 130°–150°E (Fig. 9a). During this period a downward Ekman pumping velocity is found in the western and central Pacific around this latitude, which is stronger west of the date line (Fig. 9b). Thus, this suggests that the amplitude of Rossby waves is enhanced by local winds in the western Pacific, and the resulting rapid increase of SSH near the western boundary causes the recovery of large southward ITF transport during this season.

These results are consistent with previous observational studies (e.g., Potemra et al. 2002). For example, Potemra et al. found that the sea level variation at Lombok Strait observed during 1996 through early 1999 is significantly correlated with the zonal wind stress in the equatorial Pacific at a time lag of 120 days and the maximum correlation is found around 160°E–180° north of the equator. This suggests the significant contribution of the wind forcing in the northern tropical western Pacific to the ITF seasonal variation, which is demonstrated in HYCOM experiments described above.

In addition to equatorial Rossby waves, previous studies (e.g., White et al. 2003; McClean et al. 2005) suggest that off-equatorial Rossby waves significantly influence the ITF interannual variation. For example, McClean et al. (2005) suggest that low-frequency off-equatorial Rossby waves associated with ENSO warm events may contribute to the ITF transport using a global eddy-permitting model validated by comparison to data. Our analysis does not show clear evidence for a contribution of variability north of 10°N to the seasonal cycle of ITF transport (not shown). This suggests that processes that control low-frequency ITF transport variability largely depend on the time scale. For example, the large variation of Mindanao eddies associated with ENSO (e.g., Tozuka et al. 2002; Shinoda et al. 2011) might impact interannual variability of the ITF transport, although it may not be crucial for the seasonal ITF variation.

4) Model experiment with constant Pacific winds

The analysis of the Indo-Pacific HYCOM experiment suggests the importance of the seasonal Pacific wind variation to the ITF seasonal cycle during January–March. This is evident in the ocean response within the tropical Pacific, which propagates westward as Rossby waves. To isolate the effect of the Pacific wind variation, an additional model experiment was conducted. The Indo-Pacific HYCOM was integrated with climatological wind stress that is constant in time over the Pacific (gray areas in Fig. 10a) and has the same 3-day-mean wind stress over the Indian Ocean used in the first experiment. Note that winds are also constant over the Indonesian seas for this experiment.

The transport at Makassar Strait, calculated from the two experiments, is shown in Fig. 10b. The black line indicates the total transport from the model experiment described in section 2 (referred to as a control experiment in the figure), which is same as the time series shown in Fig. 4b. The gray line is the time series of the total

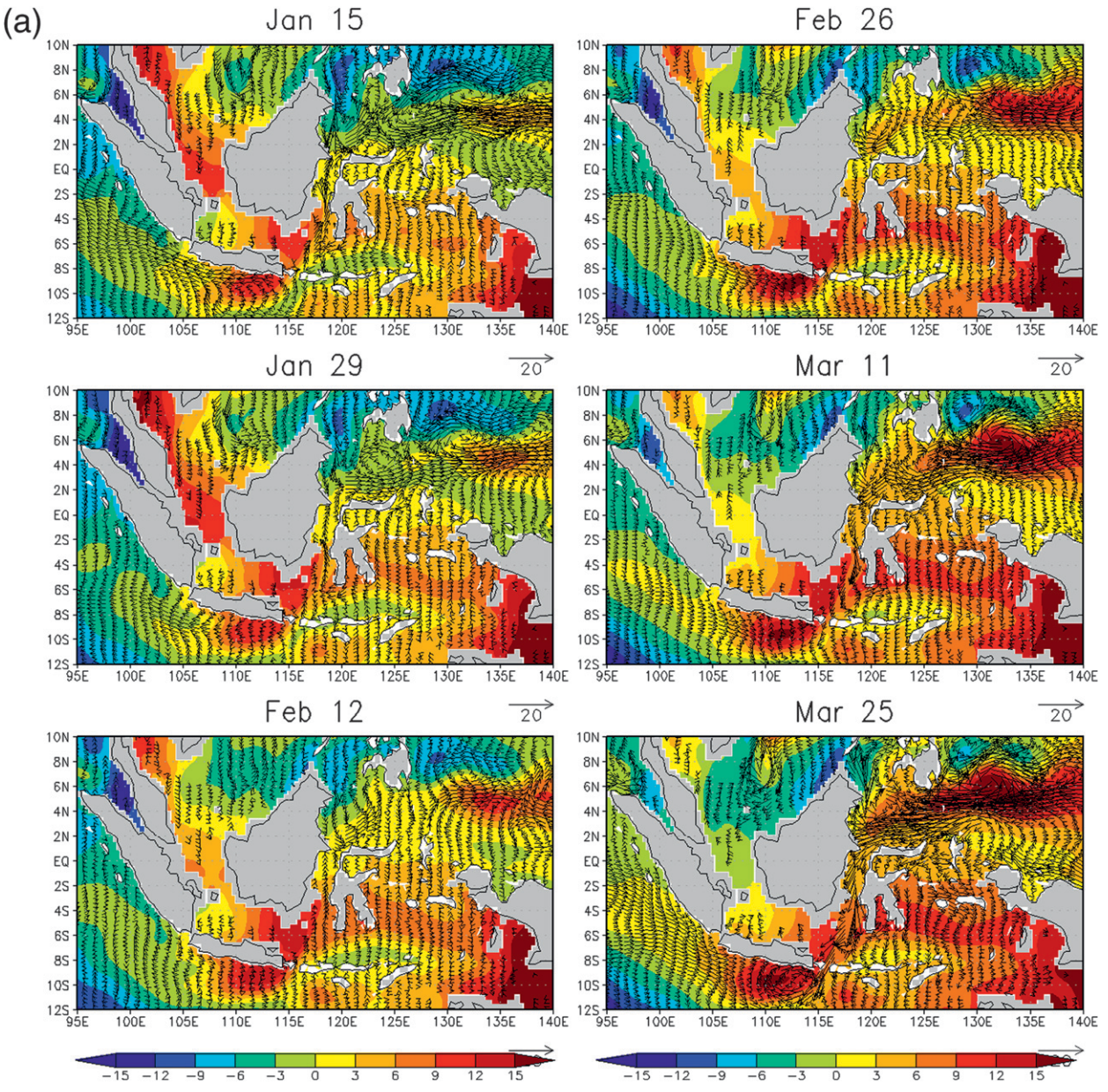

FIG. 8. (a),(b) As in Figs. 5a,b but for a different domain and time period, 15 Jan–25 Mar 2005, and the anomalies are relative to the January–March mean: color scales in (a) and (b) are different. (c) As in Fig. 5c but for a different domain and time period, 28 Jan–19 Mar 2005, and (d) as in Fig. 5d but for a different domain and time period, 20 Feb–12 Mar 2005.

transport from the experiment forced with constant Pacific winds. The reduction in southward currents at Makassar Strait during October–November is evident in both experiments. However, the subsequent recovery during January–March is not found in the experiment with constant Pacific winds (Fig. 10b). This result confirms the importance of Pacific wind variation to the ITF seasonal cycle during January–March and it shows that accurate wind forcing in the equatorial Pacific is crucial for simulating the ITF transport variability during this season.

Although the reduction of ITF transport during October–November in both experiments confirms the role of Kelvin waves from the Indian Ocean, the experiment with constant Pacific winds does not show the ITF reduction during April–May. The difference in local winds in the two experiments does not fully explain the different variation of ITF transport in the two experiments during this period. During April–May the transition from the northwest to southeast monsoon is observed in the Indonesian seas. The Ekman transport

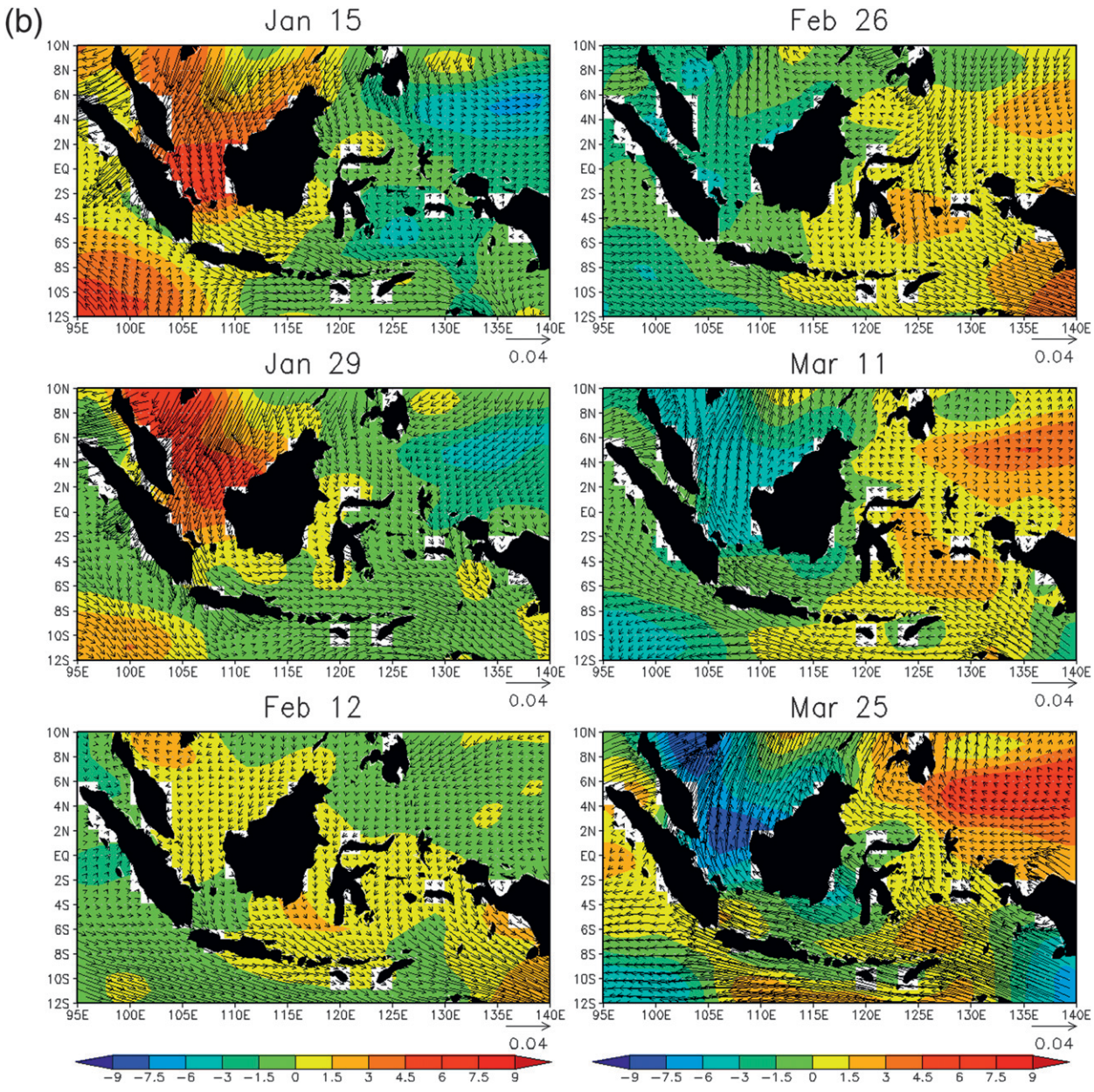

FIG. 8. (*Continued*)

at Makassar Strait is northward in early April and then becomes southward during mid-April–May. Thus, the difference between the two experiments during April could be partly due to the local winds, which tend to reduce the ITF transport. However, during May even larger ITF reduction occurs in the control experiment. Thus, the difference between the two experiments is not explained by the influence of local winds.

One possibility for the difference during May is that the difference in ocean state between the two experiments, generated during January–March, influences the subsequent Kelvin wave propagation. As discussed in this section, the propagation of annual Rossby waves makes southward ITF stronger during January–March in the control experiment. This may generate stronger convergence of currents in the Indian Ocean near Lombok Strait. As a result, the SSH around Lombok Strait relative to Makassar Strait is changed. This does not occur for the constant Pacific wind experiment because of the absence of annual Rossby waves in the Pacific. The resulting difference in the north–south pressure

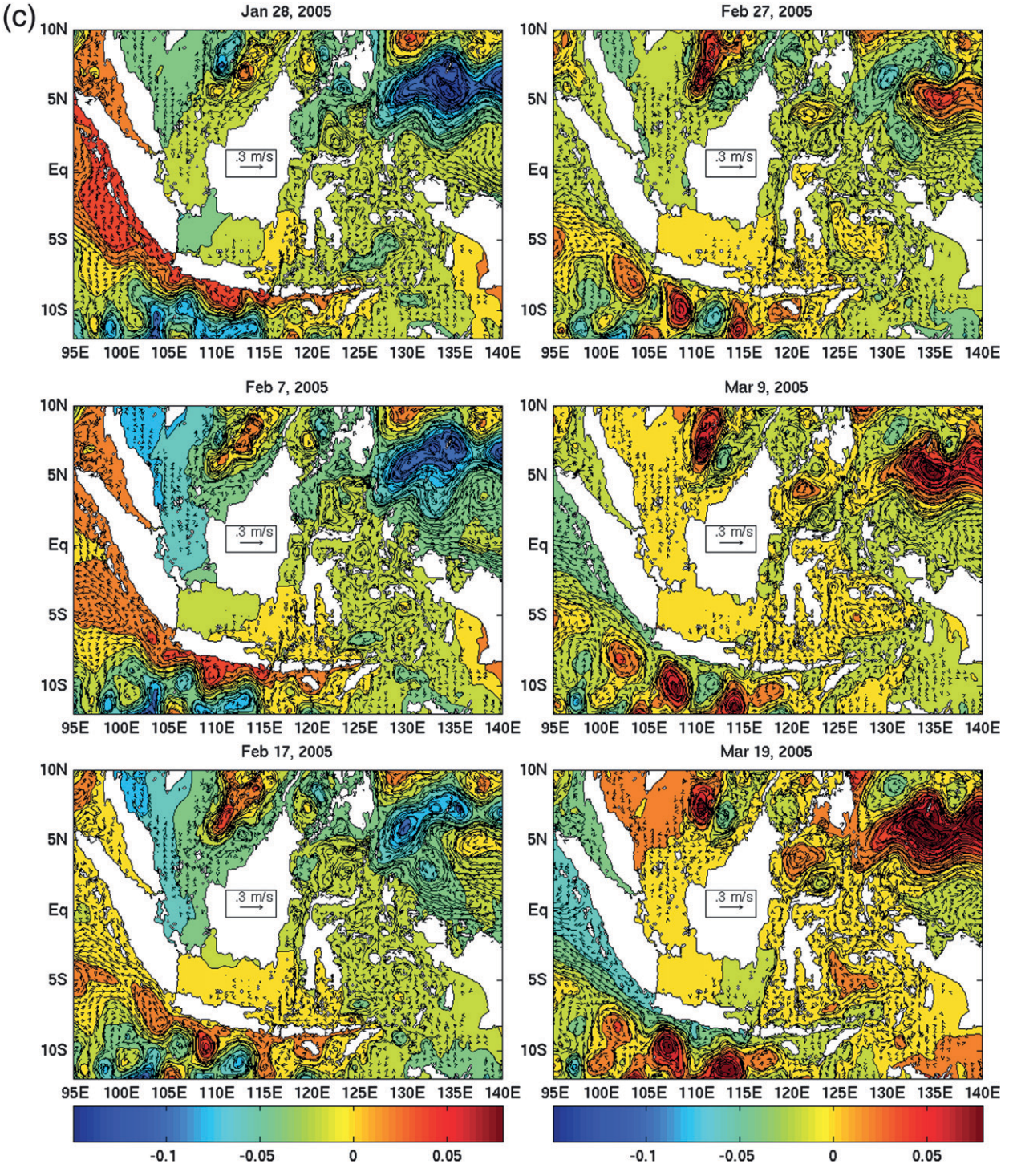

FIG. 8. (*Continued*)

gradient in the southern part of the Indonesian seas may act to reduce the amplitude of Kelvin waves between Lombok and Makassar in the constant Pacific wind experiment.

A large-scale pressure difference between the eastern Indian Ocean and western Pacific associated with the seasonal variation of ITF transport is further investigated by describing SSH variability in both basins.

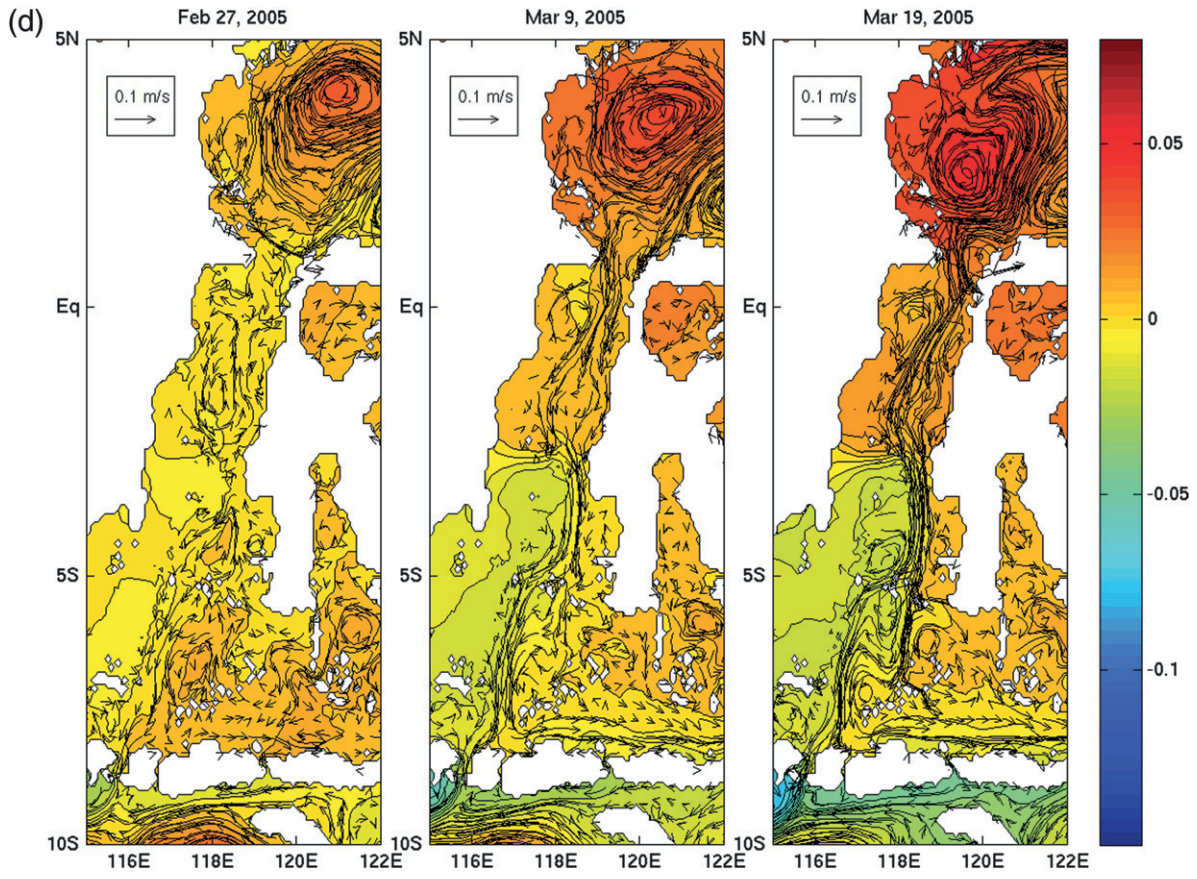

FIG. 8. (*Continued*)

Figure 11a shows the seasonal cycle of SSH difference in the western Pacific and eastern Indian Ocean (the areas shown in Fig. 1b) from the control and constant Pacific wind experiments. The SSH difference in both experiments is similar to the time series of ITF transport shown in Fig. 10b (correlation coefficient: $r = 0.90$ for the control experiment and $r = 0.72$ for the constant Pacific wind experiment), suggesting that the large-scale pressure difference between the two basins provides the forcing that drives ITF seasonal variability (Wyrtki 1987). In the control experiment, the reduction in ITF transport during May and November is associated with the SSH increase in the eastern Indian Ocean (Fig. 11b), whereas the recovery of strong ITF during January–March is associated with the sea level increase in the Pacific (Fig. 9d). The SSH difference in the constant Pacific wind experiment does not show the rapid changes during January–March because it lacks the seasonal cycle of the Pacific winds and, thus, the downwelling Rossby waves that occur during this season.

In both experiments, the SSH in the eastern Indian Ocean shows a similar seasonal cycle that includes the SSH increase associated with the Wyrtki jet during May and November (Fig. 11b). However, there are significant differences between the two experiments. For example, the rate of SSH increase in the control experiment during January–March is larger than that in the constant Pacific wind experiment. As a result, the difference between the two experiments (dashed line in Fig. 11b) rapidly increases in March when the strong ITF through Makassar Strait is generated. This SSH difference in the eastern Indian Ocean is consistent with the mechanism for the different ITF variation between the two experiments during May discussed in this section.

4. Summary and discussion

Processes that control the seasonal variation of the ITF at Makassar Strait are investigated using a series of OGCM experiments. Both the $^1/_3°$ Indo-Pacific (55°N–55°S) HYCOM and $^1/_{12}°$ global HYCOM are able to realistically simulate ITF seasonal variations observed at INSTANT moorings. An analysis of 28 years from the Indo-Pacific HYCOM simulation indicates that the decrease in southward ITF transport during April–May and October–November results from

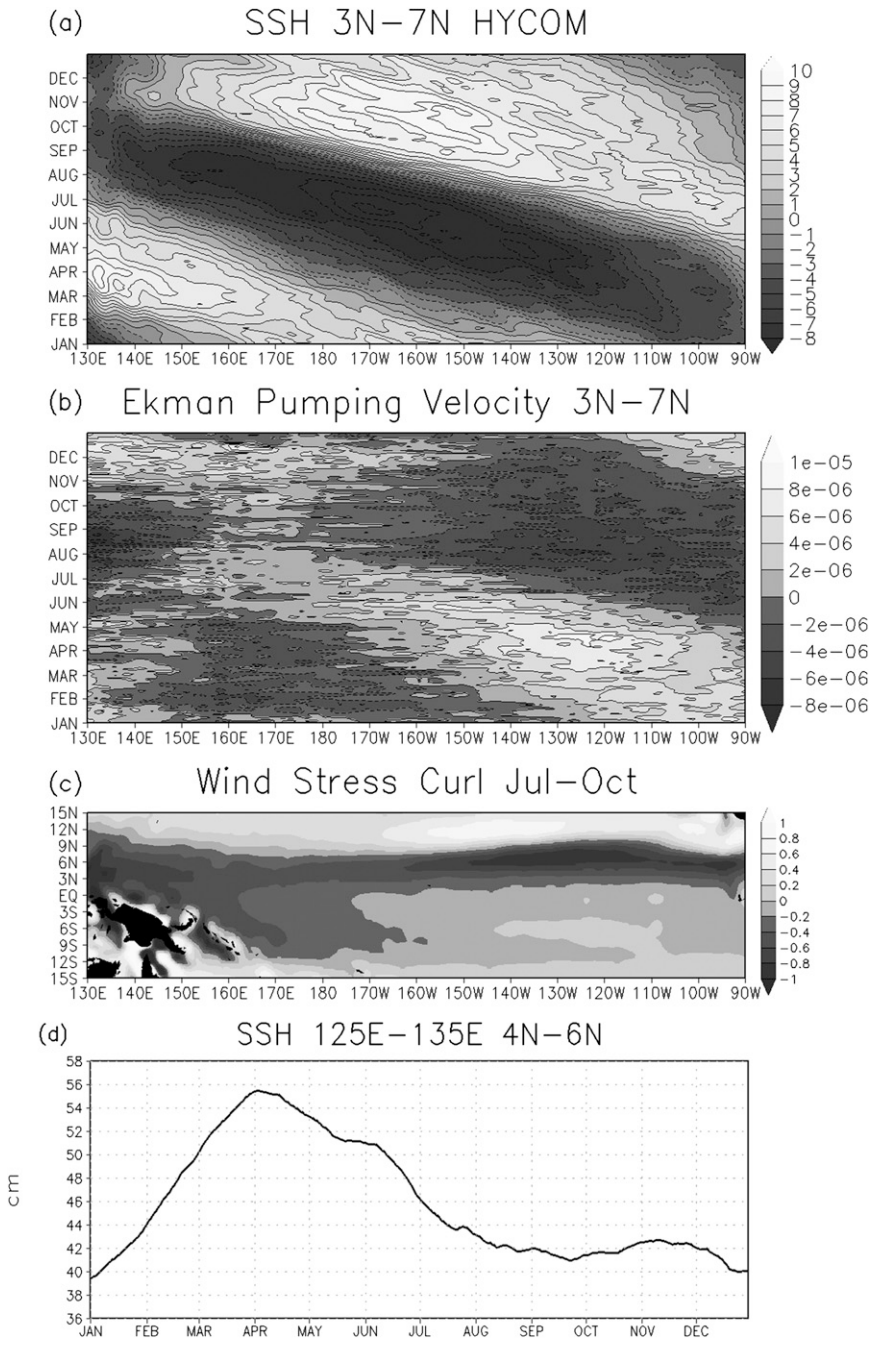

FIG. 9. (a) A longitude–time diagram of the annual cycle of the SSH anomaly at 3°–7°N from the Indo-Pacific basin HYCOM experiment and (b) as in (a) but for Ekman pumping velocity (positive upward). (c) Wind stress curl during July–October. (d) SSH averaged over the area 4°–6°N, 125°–135°E.

the wind variation in the tropical Indian Ocean through the generation of a Wyrtki jet and propagation of coastal Kelvin waves, whereas the subsequent recovery during January–March originates from seasonal upper-ocean variability associated with annual Rossby waves in the Pacific. These processes, found in Indo-Pacific HYCOM experiments, are consistent with the analysis of the global HYCOM simulation during the period of the INSTANT observations. The analysis also suggests that local wind variations along the coasts of Sumatra and Java in the Indian Ocean and the western Pacific around 5°N significantly contribute to the seasonal cycle of ITF transport.

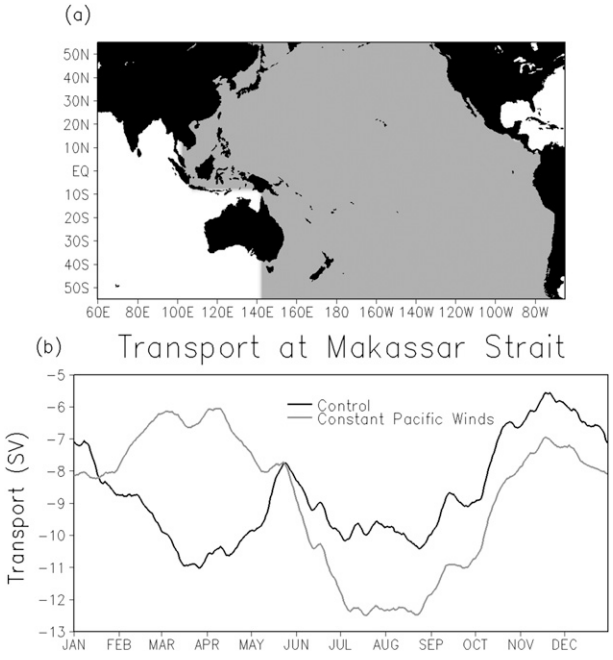

FIG. 10. (a) Map indicating the area (gray shading) where the wind stress is the long-term annual-mean climatology for the Indo-Pacific basin HYCOM experiment. (b) Seasonal cycle of total transport at Makassar Strait from the control experiment (black line) and the experiment where the Pacific wind stress is constant (gray line).

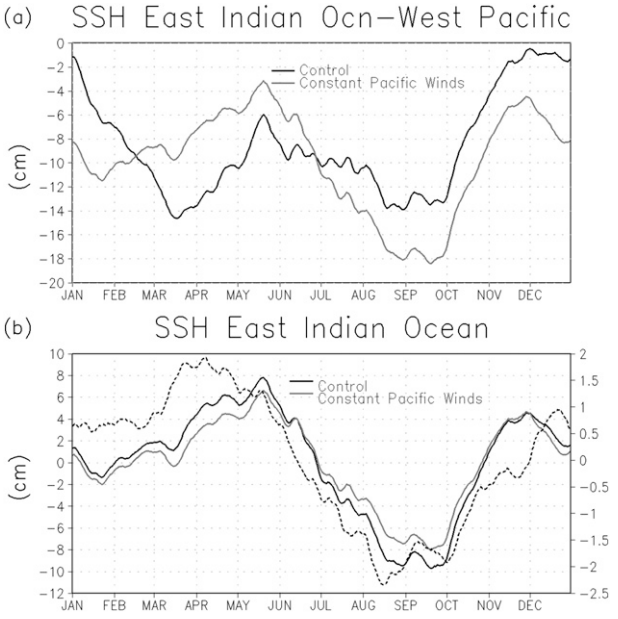

FIG. 11. (a) Seasonal cycle of SSH difference between the eastern Indian Ocean along the coast of Sumatra and Java (shown in the white box in Fig. 1b) and the western Pacific (4°–6°N, 125°–135°E) from the Indo-Pacific basin HYCOM experiment. Positive values indicate SSH in the western Pacific is higher: black (gray) lines indicate time series from the control (constant Pacific winds) experiment. (b) As in (a) but depicting the seasonal cycle of SSH in the eastern Indian Ocean. The annual means are subtracted from the time series. The dashed line shows the difference in two curves, in which positive values indicate higher SSH in the control experiment. The ordinate on the right side indicates values for the dashed line.

To isolate the effect of the Pacific wind variability on the ITF variation, an additional model experiment was conducted. The model was forced with annual-mean climatological wind stress in the Pacific and 3-day mean wind stresses in the Indian Ocean, which are same as in the first experiment. Although the reduction in southward currents at Makassar Strait during October–November is evident in this experiment, the subsequent recovery during January–March is not found. The results of this experiment confirm the relative importance of wind variations in the Pacific and Indian Ocean in each season identified by analysis of the first experiment.

Previous studies suggested that ITF transport could be estimated from sea level differences between the western Pacific and eastern Indian Ocean (e.g., Wyrtki 1987, Potemra et al. 1997). The results of the analyses presented here are consistent with these studies in that the seasonal variation of ITF transport is controlled by SSH variations in the western Pacific and eastern Indian Ocean associated with the propagation of Kelvin and Rossby waves modified by local winds. While the processes that contribute to SSH variations in both the Pacific and Indian Oceans affect the ITF transport to some extent during the entire year, the dominant processes are seasonally dependent.

During January–March, the propagation of downwelling Rossby waves in the Pacific causes the rapid increase of SSH in the western Pacific that generates the seasonal southward increase in ITF transport. Although subsequent upwelling Rossby waves make the western Pacific SSH decrease after April, the variation is much slower than in the January–March season (Fig. 9). On the other hand, changes in SSH near the coast of Java associated with Kelvin waves during May and October–November occur more rapidly, and thus the influence of Indian Ocean variation on the ITF is more visible during these seasons.

After the reduction of ITF transport in May, the transport slowly increases during June–August (Fig. 4b). SSH in both the eastern Indian Ocean and western Pacific decreases during this season because of the recovery of easterlies in the equatorial Indian Ocean and upwelling Rossby waves in the Pacific (Fig. 9a). Because the rate of the decrease in the Indian Ocean is slightly larger (Figs. 9d, 11b), a pressure gradient from the western Pacific to the eastern Indian Ocean slowly increases (Fig. 11a), and thus the ITF gradually becomes stronger. Hence, processes in neither the Indian Ocean nor the Pacific Ocean are dominant in controlling ITF transport during this season.

A comparison of SSH and upper-ocean currents with the wind stress suggests that local wind variations in the

western Pacific and eastern Indian Ocean significantly contribute to the ITF seasonal variation. In particular, changes in alongshore winds near the coasts of Sumatra and Java during October–November can greatly enhance coastal Kelvin waves that impact northward anomalous currents at Makassar Strait. Hence, accurate wind forcing in the eastern Indian Ocean near the coast as well as the proper representation of coastal processes in ocean models can improve simulations of the ITF seasonal cycle.

Alongshore winds near the coast of Sumatra and Java during October–November vary substantially on time scales that are subseasonal and interannual (e.g., Shinoda and Han 2005; Saji et al. 1999; Webster et al. 1999; Shinoda et al. 2004). Subseasonal winds can generate significant upper-ocean responses along the coast that may influence ITF transport (e.g., Iskandar et al. 2006; Schiller et al. 2010; Zhou and Murtugudde 2010). Additionally, interannual wind variations in the eastern Indian Ocean can influence ITF variations (e.g., Murtugudde et al. 1998; Masumoto 2002; Potemra and Schneider 2008). Furthermore, subseasonal wind activity in this region is strongly influenced by interannual variability, such as the IOD (Shinoda and Han 2005). Therefore, during this season, the interaction of variability on different time scales with the seasonal cycle in the eastern Indian Ocean is expected to occur every year. Investigation of oceanic and atmospheric processes on a variety of different time scales and their interactions with the seasonal cycle near the coast of Sumatra and Java is thus needed to fully understand and predict ITF variability during this season.

Acknowledgments. The altimeter products are produced by SSALTO/DUACS and are distributed by AVISO. ITF transport time series from the INSTANT observations were provided by Arnold Gordon and Dwi Susanto. This research is supported in part by 6.1 projects, ''Dynamics of the Indonesian Throughflow and Its Remote Impact'' and ''The Influence of Atmosphere Ocean Interaction on MJO Development and Propagation'' (Program Element 601153N) and the 6.2 project ''Eddy Resolving Global Ocean Prediction including Tides'' (Program Element 602435N) sponsored by the Office of Naval Research and by the NOAA/Modeling, Analysis, Predictions and Projections (MAPP) program. Weiqing Han is supported by NASA Ocean Surface Topography Science Team Program Award NNX08AR62G and NSF CAREER Award OCE 0847605.

REFERENCES

Bleck, R., 2002: An oceanic general circulation model framed in hybrid isopycnic-Cartesian coordinates. *Ocean Modell.,* **4,** 55–88.

Chassignet, E. P., L. T. Smith, G. R. Halliwell, and R. Bleck, 2003: North Atlantic simulations with the Hybrid Coordinate Ocean Model (HYCOM): Impact of the vertical coordinate choice, reference pressure, and thermobaricity. *J. Phys. Oceanogr.,* **33,** 2504–2526.

Clarke, A. J., and X. Liu, 1993: Observations and dynamics of semiannual and annual sea levels near the eastern equatorial Indian Ocean boundary. *J. Phys. Oceanogr.,* **23,** 386–399.

Cresswell, G., A. Frische, J. Peterson, and D. Quadfasel, 1993: Circulation in the Timor Sea. *J. Geophys. Res.,* **98,** 14 379–14 389.

Drushka, K., J. Sprintall, S. T. Gille, and I. Brodjonegoro, 2010: Vertical structure of Kelvin waves in the Indonesian Throughflow exit passages. *J. Phys. Oceanogr.,* **40,** 1965–1987.

Durland, T. S., and B. Qiu, 2003: Transmission of subinertial Kelvin waves through a strait. *J. Phys. Oceanogr.,* **33,** 1337–1350.

Gordon, A. L., 2005: Oceanography of the Indonesian Seas and their throughflow. *Oceanography,* **18,** 14–27.

——, R. D. Susanto, and A. Ffield, 1999: Throughflow within Makassar Strait. *Geophys. Res. Lett.,* **26,** 3325–3328.

——, ——, and K. Vranes, 2003: Cool Indonesian Throughflow as a consequence of restricted surface layer flow. *Nature,* **425,** 824–828.

——, ——, A. Ffield, B. A. Huber, W. Pranowo, and S. Wirasantosa, 2008: Makassar Strait throughflow, 2004 to 2006. *Geophys. Res. Lett.,* **35,** L24605, doi:10.1029/2008GL036372.

Han, W., 2005: Origins and dynamics of the 90-day and 30–60-day variations in the equatorial Indian Ocean. *J. Phys. Oceanogr.,* **35,** 708–728.

——, and Coauthors, 2010: Patterns of Indian Ocean sea-level change in a warming climate. *Nat. Geosci.,* **3,** 546–550.

Hautala, S. L., J. Sprintall, J. T. Potemra, A. G. Ilahude, J. C. Chong, W. Pandoe, and N. Bray, 2001: Velocity structure and transport of the Indonesian Throughflow in the major straits restricting flow into the Indian Ocean. *J. Geophys. Res.,* **106,** 19 527–19 546.

Hurlburt, H. E., E. J. Metzger, J. Sprintall, S. N. Riedlinger, R. A. Arnone, T. Shinoda, and X. Xu, 2011: Circulation in the Philippine Archipelago simulated by 1/12° and 1/25° global HYCOM and EAS NCOM. *Oceanography,* **24,** 28–47.

Iskandar, I., T. Tozuka, H. Sasaki, Y. Masumoto, and T. Yamagata, 2006: Intraseasonal variations of surface and subsurface currents off Java as simulated in a high-resolution ocean general circulation model. *J. Geophys. Res.,* **111,** C12015, doi:10.1029/2006JC003486.

Kalnay, E., and Coauthors, 1996: The NCEP/NCAR 40-Year Reanalysis Project. *Bull. Amer. Meteor. Soc.,* **77,** 437–471.

Kara, A. B., A. J. Wallcraft, P. J. Martin, and R. L. Pauley, 2009: Optimizing surface winds using QuikSCAT measurements in the Mediterranean Sea during 2000–2006. *J. Mar. Syst.,* **78,** 119–131.

Kessler, W. S., 1990: Observations of long Rossby waves in the northern tropical Pacific. *J. Geophys. Res.,* **95** (C4), 5183–5217.

Lee, T., I. Fukumori, D. Menemenlis, Z. Xing, and L. Fu, 2002: Effects of the Indonesian Throughflow on the Pacific and Indian Oceans. *J. Phys. Oceanogr.,* **32,** 1404–1429.

Masumoto, Y., 2002: Effects of interannual variability in the eastern Indian Ocean on the Indonesian throughflow. *J. Oceanogr.,* **58,** 175–182.

——, and T. Yamagata, 1993: Simulated seasonal circulation in the Indonesian Seas. *J. Geophys. Res.,* **98** (C7), 12 501–12 509.

McClean, J. L., D. P. Ivanova, and J. Sprintall, 2005: Remote origins of interannual variability in the Indonesian Throughflow region from data and a global Parallel Ocean Program simulation. *J. Geophys. Res.,* **110,** C10013, doi:10.1029/2004JC002477.

Metzger, E. J., H. E. Hurlburt, X. Xu, J. F. Shriver, A. L. Gordon, J. Sprintall, R. D. Susanto, and H. M. van Aken, 2010: Simulated and observed circulation in the Indonesian Seas: 1/12° global HYCOM and INSTANT observations. *Dyn. Atmos. Oceans,* **50,** 275–300, doi:10.1016/j.dynatmoce.2010.04.002.

Meyers, G., 1979: On the annual Rossby wave in the tropical North Pacific Ocean. *J. Phys. Oceanogr.,* **9,** 663–674.

Molcard, R., M. Fieux, and A. G. Ilahude, 1996: The Indo–Pacific throughflow in the Timor Passage. *J. Geophys. Res.,* **101,** 12 411–12 420.

——, ——, and F. Syamsudin, 2001: The throughflow within Ombai Strait. *Deep-Sea Res.,* **48,** 1237–1253.

Moore, D. W., and J. P. McCreary, 1990: Excitation of intermediate-frequency equatorial waves at a western boundary: With application to observations from the western Indian Ocean. *J. Geophys. Res.,* **95,** 5219–5231.

Murray, S. P., and D. Arief, 1988: Throughflow into the Indian Ocean through the Lombok Strait, January 1985–January 1986. *Nature,* **333,** 444–447.

Murtugudde, R., A. J. Busalacchi, and J. Beauchamp, 1998: Seasonal-to-interannual effects of the Indonesian throughflow on the tropical Indo-Pacific basin. *J. Geophys. Res.,* **103,** 21 425–21 441.

Potemra, J. T., 1999: Seasonal variations of the Pacific to Indian Ocean throughflow. *J. Phys. Oceanogr.,* **29,** 2930–2944.

——, 2001: The potential role of equatorial Pacific winds on southern tropical Indian Ocean Rossby waves. *J. Geophys. Res.,* **106,** 2407–2422.

——, and N. Schneider, 2008: Interannual variations of the Indonesian throughflow. *J. Geophys. Res.,* **112,** C05035, doi:10.1029/2006JC003808.

——, R. Lukas, and G. Mitchum, 1997: Large-scale estimation of transport from the Pacific to the Indian Ocean. *J. Geophys. Res.,* **102,** 27 795–27 812.

——, S. L. Hautala, J. Sprintall, and W. Pandoe, 2002: Interaction between the Indonesian Seas and the Indian Ocean in observations and numerical models. *J. Phys. Oceanogr.,* **32,** 1838–1854.

Rosmond, T. E., J. Teixeira, M. Peng, T. F. Hogan, and R. Pauley, 2002: Navy Operational Global Atmospheric Prediction System (NOGAPS): Forcing for ocean models. *Oceanography,* **15,** 99–108.

Saji, N. H., B. N. Goswami, P. N. Vinayachandran, and T. Yamagata, 1999: A dipole mode in the tropical Indian Ocean. *Nature,* **401,** 360–363.

Schiller, A., S. E. Wijffels, J. Sprintall, R. Molcard, and P. R. Oke, 2010: Pathways of intraseasonal variability in the Indonesian Throughflow region. *Dyn. Atmos. Oceans,* **50,** 174–200, doi:10.1016/j.dynatmoce.2010.02.003.

Schneider, N., 1998: The Indonesian Throughflow and the global climate system. *J. Climate,* **11,** 676–689.

Shinoda, T., and W. Han, 2005: Influence of Indian Ocean dipole on atmospheric subseasonal variability. *J. Climate,* **18,** 3891–3909.

——, H. H. Hendon, and M. A. Alexander, 2004: Surface and subsurface dipole variability in the Indian Ocean and its relation with ENSO. *Deep-Sea Res.,* **51,** 619–635.

——, P. E. Roundy, and G. N. Kiladis, 2008: Variability of intraseasonal Kelvin waves in the equatorial Pacific Ocean. *J. Phys. Oceanogr.,* **38,** 921–944.

——, H. E. Hurlburt, and E. J. Metzger, 2011: Anomalous Tropical Ocean Circulation associated with La Niña Modoki. *J. Geophys. Res.,* **116,** C12001, doi:10.1029/2011JC007304.

Song, Q., G. A. Vecchi, and A. J. Rosati, 2007: The role of the Indonesian Throughflow in the Indo-Pacific climate variability in the GFDL Coupled Climate Model. *J. Climate,* **20,** 2434–2451.

Sprintall, J., A. L. Gordon, R. Murtugudde, and R. D. Susanto, 2000: A semiannual Indian Ocean forced Kelvin wave observed in the Indonesian Seas in May 1997. *J. Geophys. Res.,* **105** (C7), 17 217–17 230.

——, and Coauthors, 2004: INSTANT: A new international array to measure the Indonesian Throughflow. *Eos, Trans. Amer. Geophys. Union,* **85,** 369, doi:10.1029/2004EO390002.

——, S. Wijffels, R. Molcard and I. Jaya, 2009: Direct estimates of Indonesian Throughflow entering the Indian Ocean: 2004–2006. *J. Geophys. Res.,* **114,** C07001, doi:10.1029/2008JC005257.

Syamsudin, F., A. Kaneko, and D. B. Haidvogel, 2004: Numerical and observational estimates of Indian Ocean Kelvin wave intrusion into Lombok Strait. *Geophys. Res. Lett.,* **31,** L24307, doi:10.1029/2004GL021227.

Tilburg, C. E., H. E. Hurlburt, J. J. O'Brien, and J. F. Shriver, 2001: The dynamics of the East Australian Current system: The Tasman Front, the East Auckland Current, and the East Cape Current. *J. Phys. Oceanogr.,* **31,** 2917–2943.

Tozuka, T., T. Kagimoto, Y. Masumoto, and T. Yamagata, 2002: Simulated multiscale variations in the western tropical Pacific: The Mindanao Dome revisited. *J. Phys. Oceanogr.,* **32,** 1338–1359.

Webster, P. J., A. M. Moore, J. P. Loschnigg, and R. R. Leben, 1999: Coupled ocean–atmosphere dynamics in the Indian Ocean during 1997–1998. *Nature,* **401,** 356–360.

White, W. B., Y. M. Tourre, M. Barlow, and M. Dettinger, 2003: A delayed action oscillator shared by biennial, interannual, and decadal signals in the Pacific basin. *J. Geophys. Res.,* **108,** 3070, doi:10.1029/2002JC001490.

Wijffels, S., and G. Meyers, 2004: An intersection of oceanic waveguides: Variability in the Indonesian Throughflow region. *J. Phys. Oceanogr.,* **34,** 1232–1253.

Wyrtki, K., 1973: An equatorial jet in the Indian Ocean. *Science,* **181,** 262–264.

——, 1987: Indonesian through flow and the associated pressure gradient. *J. Geophys. Res.,* **92** (C12), 12 941–12 946.

Xie, P., and P. A. Arkin, 1996: Analyses of global monthly precipitation using gauge observations, satellite estimates, and numerical model prediction. *J. Climate,* **9,** 840–858.

Yu, Z., and J. T. Potemra, 2006: Generation mechanism for the intraseasonal variability in the Indo-Australian basin. *J. Geophys. Res.,* **111,** C01013, doi:10.1029/2005JC003023.

Yuan, D., and W. Han, 2006: Roles of equatorial waves and western boundary reflection in the seasonal circulation of the equatorial Indian Ocean. *J. Phys. Oceanogr.,* **36,** 930–944.

Zhang, Y., and Coauthors, 2004: Calculation of radiative flux profiles from the surface to top-of-atmosphere based on ISCCP and other global data sets: Refinements of the radiative transfer model and the input data. *J. Geophys. Res.,* **109,** D19105, doi:10.1029/2003JD004457.

Zhou, L., and R. Murtugudde, 2010: Influences of Madden-Julian oscillations on the eastern Indian Ocean and the maritime continent. *Dyn. Atmos. Oceans,* **50,** 257–274.